$La_{1.2}CrS_{3.2}$) and its relationship to cylindrite (ca. $FePb_3Sn_4Sb_2S_{14}$), since samples of cylindrite display a spiral morphology.[15,16] As one of the more complicated of these incommensurate structures, cylindrite may be suggestive of what is occurring in "circular $NbSe_3$", i.e., stacks of layers have a tendency to curl up into cylinders due to some sort of commensurability (or lack thereof) on a scale significantly larger than the simple unit cell. However, to the best of our knowledge and others[4,17] no polymorphs have ever been reported for $NbSe_3$. Perhaps, as in the case of o-TaS_3 and m-TaS_3[4a] or as has been suggested for $PbNb_2S_5$,[8] the chains in "circular $NbSe_3$" pack into the layers in a fashion only slightly different from traditional $NbSe_3$. It is after all not uncommon to obtain different low-dimensional systems (i.e., the condensate of clusters, chains, or layers) from similar substructures through different synthetic conditions, kinetic effects, and/or slight changes in constituents or composition.[18]

(16) Makovicky, E. *Neues Jahrb. Mineral., Abh.* **1974**, *126*, 304.
(17) Fleming, R. M., private communication.

The similar, but not identical, cylindrical phenomena reported for chrysotile[19] may also aid in further explaining "circular $NbSe_3$".

In conclusion, the occurrence of "circular $NbSe_3$" suggests either some type of polymorphism or another $NbSe_x$ phase. Perhaps, some of the answers may lie in the difficulty originally reported in the characterization of the $NbSe_x$ system, $3.0 < x < 4.5$,[20] as well as in the penetrability of Nb_2Se_9 by $NbSe_3$.

Registry No. Nb_2Se_9, 65762-16-5; $NbSe_3$, 12034-78-5.

(18) For example, we recently characterized CDW behavior in $K_3Cu_8S_6$, which, like $NbSe_3$, is a layer material composed of a chain substructure (infinite $[Cu_4S_4]^{n-}$ anions). Like the trigonal prismatic chains in certain Nb and Ta chalcogenides, the $[Cu_4S_4]^{n-}$ type chain can be found in several different systems; only the method of interchain connection varies. (a) ter Haar, L. W.; DiSalvo, F. J.; Bair, H. E.; Fleming, R. M.; Waszczak, J. V.; Hatfield, W. E. *Phys. Rev. B.* **1987**, *35*, 1932. (b) Fleming, R. M.; ter Haar, L. W.; DiSalvo, F. J. *Phys. Rev. B* **1987**, *35*, 5388.
(19) (a) Whittaker, E. J. W. *Acta Crystallogr.* **1953**, *6*, 747. (b) Whittaker, E. J. W. *Acta Crystallogr.* **1956**, *9*, 855.
(20) Selte, K.; Bjerkelund, E.; Kjekshus, A. *J. Less Common Met.* **1966**, *11*, 14.

Reviews

The Potassium Titanyl Phosphate Structure Field: A Model for New Nonlinear Optical Materials

Galen D. Stucky,* Mark L. F. Phillips, and Thurman E. Gier

Department of Chemistry, University of California, Santa Barbara, California 93106

Received June 7, 1989

Potassium titanyl phosphate (KTP) is unique in its overall qualifications for second-order nonlinear and electrooptic processes with a large hyperpolarizability, an excellent temperature window, a wide wavelength range for phase matching, and outstanding crystal stability. Until recently, only KTP and its arsenic analogue, potassium titanyl arsenate (KTA), had been structurally characterized. The structural properties of KTP make it possible to design and synthesize a large structural field (currently over 40 members) to fine-tune and modify optical properties. An unusual opportunity exists to develop a quantitative model for second-order nonlinear optic (NLO) effects that can handle large structural distortions in extended structures. Current nonlinear susceptibility models concur that the microscopic hyperpolarizability of an octahedral metal center increases with distortion of its geometry and that the Ti=O (titanyl) metal center is primarily responsible for KTP's optical nonlinearity. All models assume that bulk NLO properties can be defined in terms of local structural perturbations involving either the O–Ti–O trans bonds or the TiO_6 group, ignoring cation (K^+ in KTP) and secondary atom (P or As) contributions. Since the observed optical properties are particularly sensitive to crystal quality, this review focuses on the synthesis and ion-exchange chemistry and then considers chemical modification of the KTP structure and the consequent structural and optical implications in light of the present NLO structure/property models.

1. Prologue: Why Photons?

The possibility of studying and using "photonic" processes in which data transmission and storage are primarily initiated and executed by photons rather than electrons is an increasingly attractive alternative.[1] The motivations for this are numerous. The large bandwidths available in optical data transmission make it possible to manipulate and store visual images at a density of as high as 10^8 bits/cm^2. Third-order NLO properties can be used to greatly increase optical disk storage densities so that, for example, optical data storage may some day reduce large libraries to a few small rooms. The transmission of optical pulses on a picosecond or femtosecond rather than a nanosecond time scale adds another dimension to data processing.[2] In electronics binary states define device operation, while in photonics a "grey scale" of optical states might be accessible. The fact that fiber optics in telecommunications gives us a relatively "static" free carrier

* Author to whom correspondence should be addressed.

(1) For a recent review of these applications see: *Photonic Materials*; MRS Bulletin, XIII, No. 8, Aug 1988.
(2) Fork, R. L.; Brito-Cruz, C. H.; Becker, P. C.; Shank, C. V. *Opt. Lett.* **1987**, *12*, 483.

0897-4756/89/2801-0492$01.50/0

signal is a reflection of the fact that a light wave is not easily modulated by an electric field so that noise from extraneous electromagnetic fields is minimized. Conversely this also means modulation of the carrier light waves so that they can be used in data-transfer processes is nontrivial. An optic medium must be designed and synthesized in which the modulation or combination of photons (wave mixing) can be facilitated with design control over both the magnitude and response time of optical processes. It is here that materials chemists have a vital role to play in the definition of structure/optical property relationships.

This review deals with one particular structure field, that of $KTiOPO_4$, which provides an unusual opportunity to systematically fine-tune both structural and electronic properties over a large range so that detailed studies can be made of the relationships between electrooptic properties, chemical bonding, and small structural displacements within a single topological configuration.

2. Materials Chemistry and Nonlinear Optic Behavior: Structure/Property Relationships

The focus of research in this field is to study material properties that modify or mix light waves but do not impede them so that optimal transmission results with a minimum of undesirable absorption and light scattering. Specifically, as noted above, the purpose of the nonlinear optic material is to introduce strong coupling between the electric/magnetic fields of a primary light wave and the secondary fields from another source. The latter may originate from externally applied electric/magnetic fields or internally through another electromagnetic light wave.

The behavior of a light beam passing through the optical material is defined by the refractive indexes, n_{ij}. These in turn are delineated by the static (e.g., crystal structure) and dynamic (i.e., polarization) properties of the crystal electron density. Dielectric constants, ϵ_{ij}, are a measure of electronic and ionic displacements in a material at an applied electric field frequency. At optical frequencies they are also equal to n_{ij}^2, the square of the refractive index. Our control over the optical behavior of our primary light wave by the secondary electric field can be expressed as

$$1/\mathbf{n}_{ij}^2 = 1/n_{ij}^2 + r_{ijk}E_k + s_{ijkl}E_kE_l + \ldots \quad (1)$$

where $\mathbf{n}_{ij}$ = the induced refractive indexes, n_{ij} = the refractive index in the absence of the electric field, r_{ijk} = the linear or Pockels coefficients, and s_{ijkl} = the quadratic or Kerr coefficients. Electrooptic coefficients are frequently defined in terms of r_{ijk}.[3]

Equation 1 tells us *at the bulk macroscopic level* how to couple our light wave with an applied electric field. As chemists, we are interested in what these coefficients mean in terms of the distribution and polarization of electron density. This relationship between electron polarizability and atomic structure on one hand and the behavior of light on the other is fundamental to our understanding of how chemistry can be used to synthesize and modify photonic materials. A brief overview of the details of this interaction follows.

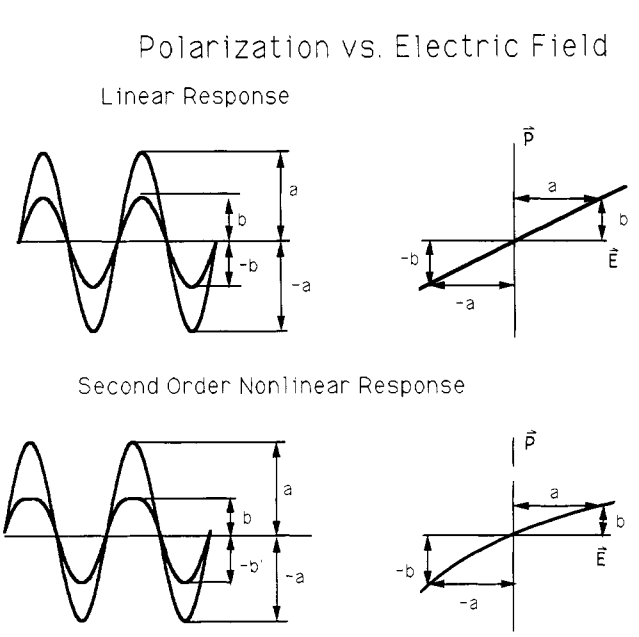

Figure 1. Linear and nonlinear polarization response in an oscillating electric field. Phase displacement of the polarization wave relative to the electric field is not shown for clarity. a and b refer to the electric field and polarization waves, respectively.

1. Nonlinear Optics and Atoms. In an optical medium, electrons are displaced by the oscillating electric field, **E**, of an incident light wave. The movement of the electrons will be determined by (1) the direction and magnitude of the electric field,[4] (2) the nature of the potential well in which the electrons reside, and (3) the frequency of the applied field (Figure 1). For linear optical effects, the harmonic displacement (polarization) of the electrons is directly proportional to the electric field as expected for a simple harmonic oscillator:

$$\mu = \alpha\mathbf{F} \quad (2)$$

If the electrons are in an effective anharmonic potential as in a dipolar bond, polarization of the electrons will be nonlinear:

$$\mu = \mu_0 + \alpha\mathbf{F} + (\beta/2)\mathbf{F}\cdot\mathbf{F} + (\gamma/6)\mathbf{F}\cdot\mathbf{F}\cdot\mathbf{F} + \ldots \quad (3)$$

Physically this is a statement that higher order nonlinear terms such as β are a measure of the potential well anharmonicity. The greater the anharmonicity of the potential well, the greater the expected nonlinear polarizability and the larger the expected nonlinear optic coefficients.[5] If the valence electrons are localized and can be

(3) Because the indices i and j of r_{ijk} can be permuted in a lossless medium, a contracted notation r_{mk} is used, where the relation between m and (ij) is given by the following: $1 \rightarrow (11)$, $2 \rightarrow (22)$, $3 \rightarrow (33)$, $4 \rightarrow (23,32)$, $5 \rightarrow (13,31)$, and $6 \rightarrow (12,21)$. The *second-order* NLO coefficient, $\chi^{(2)}_{ijk}(-\omega_\gamma;\omega_\alpha;\omega_\beta)$ for combining two photons is defined in terms of the r_{ijk} coefficients of eq 1 by

$$2\chi^{(2)}_{ijk}(-\omega_\gamma;\omega_\alpha;\omega_\beta) = -\epsilon_{ii}(\omega_\alpha)\ \epsilon_{jj}(\omega_\beta)\ r_{ijk}(-\omega_\gamma;\omega_\alpha;\omega_\beta)$$

where ω_α, ω_β, $\omega_\gamma = \omega_\alpha + \omega_\beta$ are the photon frequencies and ϵ_{ii}, ϵ_{jj} are the dielectric constant coefficients. The interested reader is referred to: Kaminow, I. P. *An Introduction to Electrooptic Devices*; Academic Press: New York, 1974.

(4) The electric field that the electron feels is actually made up of contributions from applied field, **E**, and the internal electric fi d of the media. The linear polarization is then given by $\alpha\mathbf{F}$, where $\mathbf{F} = \mathbf{N}\cdot\mathbf{E}$, and **N** is a tensor that defines the orientation of the local field at the molecule or bond of interest.

(5) Using thermodynamic arguments, Miller first noted this physical picture of NLO in 1964. In this model, the second-order coefficient

$$\chi^{(2)}_{ijk}(-\omega_\gamma;\omega_\alpha;\omega_\beta) = \chi_{ii}(\omega_\gamma)\ \chi_{jj}(\omega_\alpha)\ \chi_{kk}(\omega_\beta)\ \Delta_{ijk}$$

with Δ_{ijk} = (constant)(anharmonic potential). The Δ_{ijk} values that define the anharmonic potentials are surprisingly constant so that one can get a rough estimate of the second-order average NLO coefficient from first-order susceptibilities, i.e., the linear polarizabilities. But since the optical linear polarizabilities are explicitly given by the indexes of refraction, straightforward optical microscopy measurements give the desired estimate. See: Miller, R. C. *Appl. Phys. Lett.* **1964**, *5*, 17. Kurtz, S. K. *Laser Handbook*; Arecchi, F. T., Schulz-Dubois, E. O., Eds.; North Holland: Amsterdam, 1972; Vol. 1, p 923.

assigned to specific bonds, β is referred to as the bond polarizability. If the valence electron distribution is delocalized as in organic aromatic or acetylenic molecules, β can be described in terms of molecular polarizability. Intuitively one would expect that if the effective potential well is delocalized over several atom sites, the polarizability and nonlinear optic coefficients would be larger. This is indeed the case as evidenced by the fact that the largest NLO coefficients are found for semiconductors and unsaturated extended organic molecules.[6] In summary, eq 3 describes the polarization at the atomic level where first-order (α), second-order (β), etc., harmonic coefficients are defined in terms of bond and molecular polarizabilities. μ is then the net bond or molecular polarization.

The observed bulk polarization is given by an expression analogous to (3):

$$\mathbf{P} = \mathbf{P}_0 + \chi^{(1)}\mathbf{E} + \chi^{(2)}\mathbf{E}\cdot\mathbf{E} + \chi^{(3)}\mathbf{E}\cdot\mathbf{E}\cdot\mathbf{E} + \ldots \quad (4)$$

where the $\chi^{(i)}$ susceptibility coefficients are tensors. $\mathbf{P}_0$ is the built-in static dipole of the sample, which might consist of a collection of molecules in a glass, a ferroelectric liquid crystal, or a noncentrosymmetric crystal. If the atoms are part of a centrosymmetric crystal, then

$$\mathbf{P}(\mathbf{E}) = -\mathbf{P}(-\mathbf{E}) \quad (5)$$

so that the even-order terms vanish and no second-order harmonic term is observed. The reader can picture eq 4 as a polarization wave consisting of the charge displacements induced by the electromagnetic field of the incident light wave.

The induced electronic charge displacement within the medium acts as a classical oscillating dipole and emits a photon. For linear first order polarization the radiation has the same frequency as the incident light. If the polarization is nonlinear, then frequencies can be doubled, tripled, etc. As might be expected, the magnitude of the coefficients of the terms in eq 4 diminishes rapidly at higher orders. Frequency doubling is referred to as a three-wave mixing process, since the net effect is that two photons with frequency ω have combined to generate a single photon with frequency 2ω. To do this efficiently, conditions must be arranged so that the light waves propagate in phase synchronization (phase matching). This means that the group velocities and hence the refractive indexes experienced by the interacting waves as they propagate through the medium must match, e.g., $n(\omega) = n(2\omega)$. The phase-matching ability is a critical property that is an important figure of merit parameter for nonlinear optic material synthesis and design.

Second harmonic generation, or SHG, has already seen widespread applicability in laser frequency conversion, especially for the powerful Nd:YAG laser, as have other second-order processes, such as sum-and-difference frequency mixing and optical parametric oscillation. A fourth process, the Pockels effect, is used in electrooptic switching or modulation, where the refractive index of the medium is altered by an externally applied electric field.

2. Summary. Phenomenologically, the coupling between electromagnetic waves or primary wave and signal within the optical medium can be summarized as follows: (1) the electromagnetic wave with frequency ω_a generates a polarization of the electron density within the crystal, a *polarization wave*; (2) an applied electric field will modulate the polarization wave and the corresponding transmitted light wave; (3) alternatively in a nonlinear medium, the polarization wave may contain higher frequency harmonics, effectively coupling two or more photons of the primary electromagnetic radiation to generate light of frequency $2\omega_a$, $3\omega_a$, etc., or (4) a second primary wave with frequency ω_b might be introduced to give a new polarization wave that reemits radiation at the sum and difference frequencies, $\omega_a + \omega_b$ and $\omega_a - \omega_b$. Other wave-mixing combinations are possible for higher order harmonics.

Another description of the microscopic behavior can be given in terms of quantum mechanical mixing of ground and excited states via perturbation of the ground-state electron density.[7] An application of this approach is discussed below in conjunction with studies of structure/property relationships.

(6) See: Williams, D. J. *Angew. Chem., Int. Ed. Engl.* **1984**, *23*, 690, and included references.

Table I. Lattice Constants of KTP Synthesized by Various Techniques

prep method	a, Å	b, Å	c, Å	ref
hydrothermal	12.8157	6.4027	10.5866	40
flux	12.814	6.404	10.616	15
flux	12.83	6.41	10.61	31
tungstate flux	12.840	6.396	10.584	43
gel growth	12.821	6.416	10.574	45

3. Potassium Titanyl Phosphate (KTP)

Since it was introduced as a nonlinear optical material in 1976,[8] potassium titanyl phosphate ($KTiOPO_4$, or KTP) has received considerable attention as a medium in applications requiring a high degree of second-order susceptibility. KTP has been recognized as the material of choice for second harmonic generation, or SHG, of Nd:YAG light, due to its extremely low onset power threshold,[9] high power conversion efficiency, and high threshold to laser-induced damage.[10] It has also been the focus of considerable attention for optical parametric oscillation,[11] sum and difference frequency mixing,[12] and electrooptic switching, where it is potentially competitive with Ti-doped $LiNbO_3$ wave guides.[13] This review will first examine the relationship between the parent KTP's structural and electrooptic properties and discuss them in the context of existing and future device requirements. Synthetic routes to KTP will be described, and the merits and disadvantages of each weighed. Methods of permuting the KTP structure to yield a large number of compositional and structural variations will be demonstrated. The balance of the review will explore the compositional phase space of the KTP field in the context of understanding the relationships between nonlinear optic properties, composition, and external environment, e.g., temperature and pressure.

1. Structure. The first account of the synthesis of $KTiOPO_4$ was published in 1890 by Ouvrard,[14] who prepared crystals by dissolving TiO_2 in a flux containing potassium orthophosphate and pyrophosphate and then cooling the resulting melt. The resulting crystals were "biaxial, slightly birefringent, and apparently monoclinic". Lattice parameters were measured for KTP, $RbTiOPO_4$

(7) Meredith, G. R. *Mater. Res. Bull.* **1988**, *13*, 24.
(8) Zumsteg, F. C.; Bierlein, J. D.; Gier, T. E. *J. Appl. Phys.* **1976**, *47*, 4980.
(9) Eimerl, D. *Proc. SPIE—Int. Soc. Opt. Eng.* **1986**, *681*, 5.
(10) Fan, T. Y.; Huang, C. E.; Hu, B. Q.; Eckhardt, R. C.; Fan, Y. X.; Byer, R. L.; Feigelson, R. S. *Appl. Opt.* **1987**, *26*, 2391.
(11) Vanherzeele, H.; Bierlein, J. D.; Zumsteg, F. C. *Appl. Opt.* **1988**, *27*, 3314.
(12) (a) Baumert, J. C.; Schellenberg, F. M.; Lenth, W.; Risk, W. P.; Bjorklund, G. C. *Appl. Phys. Lett.* **1987**, *51*, 2192. (b) Risk, W. P.; Baumert, J. C.; Bjorklund, G. C.; Schellenberg, F. M.; Lenth, W. *Appl. Phys. Lett.* **1988**, *52*, 85.
(13) Bierlein, J. D.; Ferretti, A.; Brixner, L.; Hsu, Y. *Appl. Phys. Lett.* **1987**, *50*, 1216–8.
(14) Ouvrard, L. *Compt. Rend.* **1890**, *121*, 117.

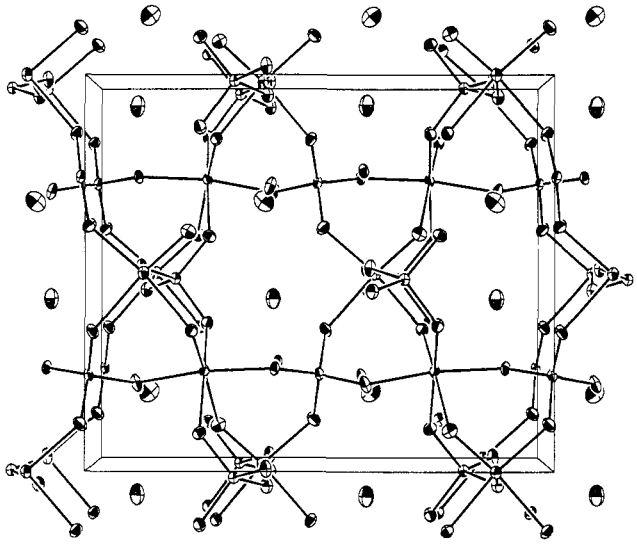

$KTiOPO_4$ Orthorhombic $Pna2_1$

Figure 2. View of KTP unit cell along the [010] direction. Cations migrate through channels parallel to [001].

(RbTP), and $TlTiOPO_4$ (TlTP) by Masse and Grenier in 1971,[15] and the crystal structure of KTP was determined by Tordjman et al. in 1974.[16]

Like all crystalline phases that show second-order nonlinearity, KTP is acentric. It belongs to the orthorhombic space group $Pna2_1$, with a = 12.814 Å, b = 6.404 Å, c = 10.616 Å, and V_{cell} = 871.16 Å^3.[15] These cell dimensions are not invariant but depend on the method by which KTP is prepared (Table I). There are four asymmetric units per unit cell, and two formula units per asymmetric unit. There are therefore two different K sites, as well as two different Ti and P sites. Because both sets of atoms in the asymmetric unit are in general positions, the KTP structure is extremely versatile, and many isomorphic derivatives can be obtained by permuting the constituent elements (Table VII). The framework is characterized by TiO_6 chains linked by phosphate bridges (Figure 2). The open nature of this framework allows cations to diffuse easily parallel to [001], which is also the polar axis.[13] This ease of diffusion results in a relatively large, and highly anisotropic, ionic conductivity in KTP and allows both ion exchange[17] and gas-phase desorption and resorption to take place.[18]

The earliest localized bond polarization models[19] have noted that unequal trans-metal–oxygen bond lengths can result in substantially different bond polarizabilities. Since these contribute to dipolar displacements in opposite directions, the result is a large net contribution to the second-order nonlinear susceptibility (see section 4).[20] In KTP, O–Ti–O units link as trans for one of the two structurally independent titanium atoms and cis for the other titanium atom to form a helical chain along [011]. For each titanium atom there is a short (<1.75 Å) "titanyl" Ti–O bond trans to a long (>2.10 Å) Ti–O bond. This long bond is to a titanyl oxygen atom (O(10) in Figure 3) in the

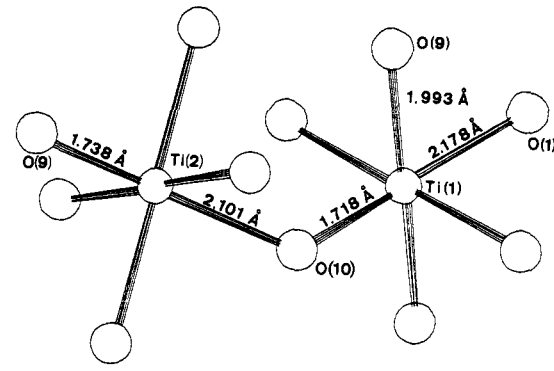

Figure 3. Ti coordination environment in KTP asymmetric unit.

trans-Ti–O linkage and to a phosphate oxygen atom (O(1) in Figure 3) in the cis-titanyl linkage.[16] For the KTP isostructures described in this review, these distances can be highly asymmetric with bond-length differences exceeding 0.50 Å. Adding one d electron to the octahedral t_{2g} orbital set in $KVOPO_4$ does not substantially change the asymmetry of the trans-M–O bond distances[21] (Table VIII). Similar distortions from perfect octahedral symmetry exist in other ferroelectrics, such as $LiNbO_3$, $Ba_2NaNb_5O_{15}$, and $LiTaO_3$.[20] This feature is clearly important in understanding structure/property relationships in the SHG response of the KTP structural family.

2. Optical Properties. An excellent review describing the optical properties and new applications of KTP crystals in devices has been recently published by Bierlein and Vanherzeele.[22] KTP's utility as a doubling material rests not only on its large nonlinear optic coefficients but also on its optical transparency in the visible and near-IR regions and its phase-matching limits. For phase matching to occur, there must be some angle of incidence through the crystal for which both the fundamental and second harmonic photons experience the same refractive index. Normal dispersion makes this a special condition: the birefringence of the crystal must be such that at some point on the surface of the refractive index ellipsoid, the phase velocities of the fundamental ordinary ray and the second harmonic extraordinary ray are identical. Biaxial and uniaxial (birefringent) crystals offer the possibility of coincidence of the phase matching direction and one of the optic axes. This highly desirable situation, called noncritical phase matching, is quite tolerant of divergence of the incident beam from the most efficient phase-matching direction. This tolerance reduces the influence of beam divergence on the phase-matching efficiency for a particular crystallographic direction.

There are two types of phase matching for SHG: type I, where the two fundamental photons are of the same polarization, and type II, where they are orthogonally polarized.[23] For KTP, type II interaction results in the most efficient phase matching. Noncritical type II phase matching occurs at two wavelengths, 990 and 1080 nm, for propagation in the x–y plane, resulting in a large acceptance angle and low walkoff (the angle by which, due to birefringence, the second harmonic beam separates from the fundamental). The type II interaction in the y–z plane is phase matchable from 990 nm to 3.5 μm, though this condition is more angle dependent than for propagation in the x–y plane. However, between 1.5 and 2.5 μm the

(15) Masse, R.; Grenier, J. C. *Bull. Soc. Fr. Mineral. Cristallogr.* **1971**, *94*, 437.
(16) Tordjman, I.; Masse, R.; Guitel, J. C. *Z. Kristallogr.* **1974**, *139*, 103.
(17) Phillips, M. L.; Gier, T. E.; Eddy, M. M.; Keder, N. L.; Stucky, G. D.; Bierlein, J. D. *Solid State Ionics* **1989**, *32/33*, 147–53.
(18) Eddy, M. M.; Gier, T. E.; Keder, N. L.; Stucky, G. D.; Cox, D. E.; Bierlein, J. D.; Jones, G. *Inorg. Chem.* **1988**, *27*, 1856.
(19) Jeggo, C. R.; Boyd, G. D. *J. Appl. Phys.* **1970**, *41*, 2741.
(20) Levine, B. F. *Phys. Rev. B* **1973**, *7*, 2600–2625.
(21) Harrison, W. T. A.; Phillips, M. L.; Gier, T. E.; Keder, N. L.; Stucky, G. D., manuscript submitted for publication.
(22) Bierlein, J. D.; Vanherzeele, H. *J. Opt. Soc. Am. B* **1989**, *6*, 622–633.
(23) Belt, R. F.; Gashurov, G.; Liu, Y. S. *Laser Focus* **1985**, 110.

Table II. Refractive Indexes of KTP and KTA Synthesized by Various Techniques at 1.064 μm

compd	prep method	N_x	N_y	N_z	ref
KTP	hydrothermal	1.740	1.7469	1.8304	23
KTP	flux	1.7381	1.7458	1.8302	10
KTP	tungstate flux	1.740	1.743	1.830	43
KTA	tungstate flux	1.782	1.790	1.868	30

phase-matching angle is nearly constant in both the x–z and y–z planes, and this results in wavelength-noncritical phase matching.

KTP's principal success as a nonlinear optic medium lies in the nearly unparalleled efficiency of its type II doubling of Nd:YAG laser light at 1064 nm. Other second-order wave-mixing processes demonstrated in KTP include sum-frequency generation (SFG) and optical parametric oscillation (OPO). SFG occurs when two photons of frequency ω_1 and ω_2 combine to give a third photon with a frequency ω_3 such that $\omega_3 = \omega_1 + \omega_2$. SHG is thus a special case of SFG, where $\omega_1 = \omega_2$. Optical parametric oscillation can be viewed as the reverse of the SFG process. Pump photons decay into signal and idler photons such that $\omega_p = \omega_s + \omega_i$. The frequencies ω_s and ω_i are determined by the phase-matching condition: the momenta ($\mathbf{k}$) of the signal, idler, and pump waves must be such that $\mathbf{k}_p = \mathbf{k}_s + \mathbf{k}_i$. Output tuning is thus accomplished by altering the refractive indexes experienced by ω_p, ω_s, and ω_i. For oscillation to occur, ω_s and ω_i must change to meet the criterion $\Delta\mathbf{k} = 0$, i.e., phase matching of pump and output beams. The phase matching condition may be altered by changing incident angle or temperature or by applying an external potential (electrooptic tuning).[24] This refractive index tuning is an example of the Pockels effect. Like its cell dimensions, KTP's principal indexes depend on the route by which it was synthesized (Table II). These variations in refractive index can affect the angle at which phase matching occurs.

The recent availability of improved Sellmeier equation coefficients has allowed the demonstration of optical parametric oscillation (OPO) in KTP.[11] Phase-matching angles have been experimentally determined for a type II interaction of signal and idler in the x–z and y–z planes using the 526-nm second harmonic of Nd:YLF as the pump beam. It is found from theory and from experiment that KTP's OPO output with this pump wavelength is angle tunable from 0.60 to 4.3 μm,[25] and as a result, KTP can be used as a broadly tunable near–mid-IR source, with a tunable range of 14 000 cm^{-1}. This tunability at 0.53 μm compares favorably with the ranges of other common NLO materials transparent in the visible, e.g., $LiNbO_3$, which can be angle tuned from 0.68 to 2.36 μm.[26]

KTP is noncritically phase matchable in the type II sum frequency mixing of 1064- and 809-nm light, which yields 459-nm radiation. This research illustrates another remarkable property of KTP, the large temperature window (Figure 4) over which it can be used in NLO applications.[12] Additionally, mixing of fundamental and second harmonic (cascade tripling) of Nd:YAG at 1.32 μm has been reported in KTP. This nearly angle-noncritical type II interaction results in 0.44-μm radiation, the shortest wavelength reported from KTP.[27] Third-order NLO response has been

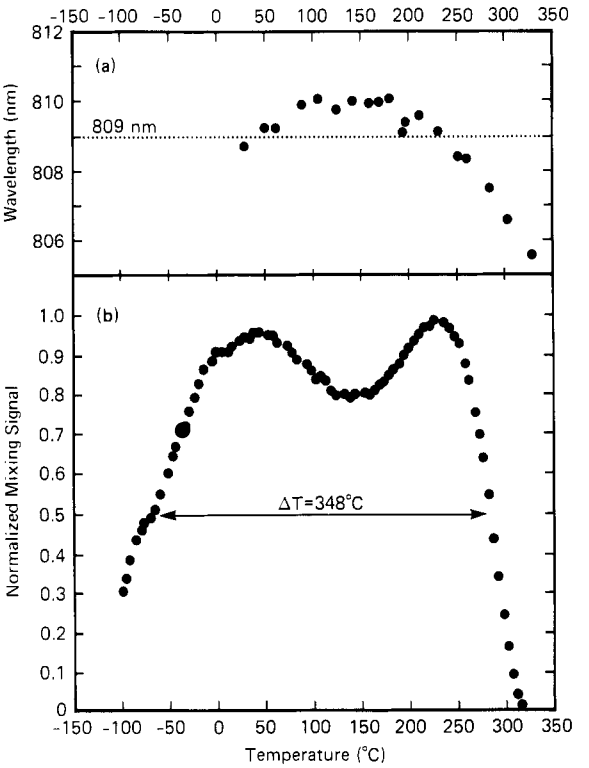

Figure 4. (a) Phase-matching wavelength vs temperature. (b) Generated sum frequency power vs temperature with dye laser wavelength held constant at 809 nm.

observed in KTP and is currently under investigation.[22]

KTP's threshold power to the type II doubling of 1.064-μm light, at 0.1 MW, is the lowest for any material on which detailed measurements have been made.[9] Its laser damage threshold, at approximately 15 GW/cm^2 for 1-ns pulses,[10] makes it applicable for high-power pulsed Nd:YAG lasers as well as continuous wave systems. This contrasts with other ferroelectric crystals such as $LiNbO_3$, which can be readily damaged even at moderate power-levels.[23]

KTP's transparency range reaches from 350 nm to 4.5 μm, and these wavelengths limit the spectral width of KTP's utility as an optical medium. The UV absorption, caused by a ligand-to-metal charge-transfer (LMCT) band, renders KTP unsuitable for sequential doubling or generation of higher order harmonics below 350 nm. These processes are also limited by loss of efficient type II phase matching. It is important, though, to remember that no single NLO material can satisfy the requirements for all possible applications, and materials should be selected on the basis of a specific need. The role of the synthetic chemist in the field of nonlinear optics is to develop new materials for new applications and enhance the inventory of materials available for existing applications. It is along these lines that the exploration of the KTP structure field proceeds.

3. Other Physical Properties. Owing to the mobility of cations through the relative open channel parallel to the c direction, KTP exhibits a moderately strong ac ionic conductivity along [001] which can vary by 4 orders of magnitude from 10^{-10} to 10^{-6} Ω^{-1} cm^{-1} at 10 Hz,[28] depending on the method of preparation (Figure 5). This conductivity is highly anisotropic, as the conductivity perpendicular to [001] is only 10^{-4} of that parallel to [001].[29] This

(24) Smith, R. G. *Laser Handbook*; Arecchi, F. T., Schulz-DuBois, E. O., Eds.; North-Holland: Amsterdam, 1972; Vol. 1, pp 839–95. The reader is referred to this chapter for a comprehensive introduction to optical parametric oscillators.

(25) The tuning range is briefly discontinuous in the x–z plane near the degeneracy condition $\omega_s = \omega_i$ (1.03 μm), where the interaction is not phase matchable.

(26) Miller, R. C.; Norland, W. A. *Appl. Phys. Lett.* **1967**, *10*, 53.

(27) Anthon, D. W.; Crowder, C. D. *Appl. Opt.* **1988**, *27*, 2650.

(28) Morris, P. A.; Crawford, M. K.; Ferretti, A.; French, R. H.; Roelofs, M. G.; Bierlein, J. D.; Brown, J. B.; Loiacono, G. M.; Gashurov, G. MRS Proceedings Book; *Optical Materials*; in press.

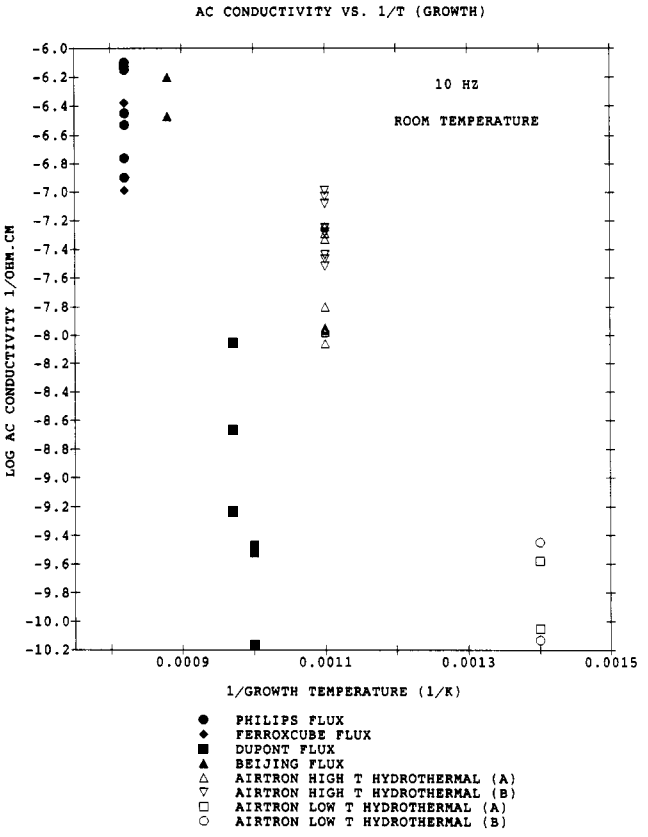

Figure 5. Ac conductivity vs reciprocal growth temperature (from ref 27).

is a particularly important property as it permits the synthesis of optical wave guides by ion exchange in KTP at relatively low temperatures with vertical optical channel walls parallel to the polar [001] axis.[13] Figure 5 also points out the importance of synthetic procedure in defining polarizabilities and other properties essential for characterizing the nonlinear optic response. Both flux and hydrothermal crystal growth procedures can result in either low or high ionic conductivities. Within the limits of the detection capabilities used, no differences were observable in the chemical impurity content of the samples shown in Figure 5.[28] The differences in conductivities are assigned to a defect model with nonstoichiometry variations on the K and O sublattices of KTP. The higher the defect concentration, the higher the conductivity *and the more susceptible KTP is to optical and electric field damage.* This is explained on the basis of compensating defect charge by varying [Ti^{3+}] concentrations. These studies are particularly important in establishing the importance of another common solid-state phenomenon, defect chemistry, in nonlinear optic materials chemistry. The conductivity in the *c* direction of $RbTiOPO_4$ is lower than that of $KTiOPO_4$ by about a factor of 100, presumably due to the decreased mobility of the larger Rb^+ ion.[13] Rather surprisingly, the conductivity of $KTiOAsO_4$ is less than that of KTP.[30]

The fact that the point group to which KTP belongs, *mm*2, is polar allows the possibility that KTP is a ferroelectric. Because of the high conductivity in the polar direction, the spontaneous polarization canot be readily measured, and KTP's ferroelectric properties cannot be thusly observed.[8] KTP's ferroelectricity was first suggested

Table III. Curie Temperatures of KTP Isostructures

compd	T_c, °C	ref
$KTiOPO_4$	934	31
$RbTiOPO_4$	789	31
$TlTiOPO_4$	581	31
$KTiOAsO_4$	880	30

by Yanovskii et al., who discovered dielectric anomalies at elevated temperatures in KTP, RbTP, and TlTP, and determined Curie temperatures for these compounds (Table III).[31] These anomalies coincide with complete and reversible losses in powder SHG intensity. From the dielectric susceptibility and SHG intensity data, Yanovskii et al. speculated that a displacive ferroelectric → paraelectric phase transition takes place, accompanied by a change of space group symmetry at the Curie temperature from $Pna2_1$ to *Pnma*. Recent high-temperature single-crystal neutron-scattering experiments on TlTP confirm that the Ti atoms are shifted toward central positions in the TiO_6 above T_c but show that the symmetry of the new lattice is *Pnan* rather than *Pnma*[32] (see section 6.1). The ferroelectric nature of KTP is verified by the observation of 180° domain walls via etching,[33] piezoelectric methods, and measurement of surface pyroelectric and bulk electrooptic properties.[34] The latter study conclusively established the ferroelectric nature of KTP via direct observation of domain switching.

KTP's ferroelectricity becomes important in its synthesis, as care must be taken to avoid growth of more than one domain in the same crystal. Precipitation of KTP from flux above the Curie temperature (936 °C) leads to crystals particularly susceptible to random multidomain structures. These in turn can lead to loss of SHG conversion efficiency and multiple SHG maxima as a function of temperature and incident angle. These temperature- and angle-tuning measurements, as well as the piezoelectric and pyroelectric techniques, have been used for screening purposes to ensure that seed crystals in hydrothermal synthesis are free of domain boundaries, which can be transmitted to the growing crystal. Poling of multidomain KTP single crystals at elevated temperatures (up to 500 °C) has yielded, in some samples, electrooptic coefficients similar to those for crystals grown as a single domain.[34]

4. Device Applications. In addition to SHG, SFG, and parametric oscillation, KTP has been employed in the fabrication of electrooptic wave guides,[13] much like those presently made in $LiNbO_3$ crystals.[35] A wave guide consists of a nonlinear optic crystal onto whose surface a dopant has been applied, forming a channel or planar region on the surface, with a refractive index greater than the surroundings. Light entering the channel is totally internally reflected by the refractive index difference between the inside and outside of the channel and can be controlled by refractive index changes induced by an applied electric field (Pockels effect). These wave guides can be used to make guided-wave devices including optical switches, modulators, and wavelength filters. An optical switch allows an input signal to be routed through either of two adjacent wave guides. The switching results from coupling of light entering one channel into the other via overlap in the evanescent fields of the two guides. The

(29) Bierlein, J. D.; Arweiler, C. B. *Appl. Phys. Lett.* **1986**, *49*, 917.
(30) Bierlein, J. D.; Vanherzeele, H.; Ballman, A. A. *Appl. Phys. Lett.* **1989**, *54*, 783.
(31) Yanovskii, V. K.; Voronkova, V. I. *Phys. Status Solidi A* **1980**, *93*, 665–8.
(32) Harrison, W. T. A.; Schultz, A. J.; Gier, T. E.; Stucky, G. D., manuscript submitted for publication.
(33) Voronkova, V. I.; Gvozdover, R. S.; Yanovskii, V. K. *Pisma Zh. Tekh. Fiz.* **1987**, *13*, 934.
(34) Bierlein, J. D.; Ahmed, F. *Appl. Phys. Lett.* **1987**, *51*, 1322.
(35) Alferness, R. C. *IEEE J. Quantum Electron.* **1981**, *QE-17*, 946.

Table IV. Electrooptic Parameters for Inorganic Materials[a]

compd	r, pm/V	n	ϵ_{eff}	n^3r/ϵ_{eff}
KTA, r_{33}	40	1.91	15	19.0
KTP, r_{33}	35	1.86	13	17.3
$KNbO_3$, r_{33}	27	2.17	30	9.2
KTA, r_{23}	21	1.81	15	8.4
$LiNbO_3$, r_{33}	29	2.20	37	8.3
$Ba_2NaNb_5O_{15}$	56	2.22	86	7.1
KTP, r_{23}	14	1.76	13	5.9
SBN (25–75)	56–1340	2.22	119–3400	5.1–0.14
GaAs	1.2	3.6	14	4.0
$LiNbO_3$, r_{13}	10	2.29	37	3.2
$BaTiO_3$	28	2.36	373	1.0

[a] Electrooptic wave guide modulator figures of merit for several inorganic materials. Adapted from: Holman, R. L. Materials and Device Issues in Guided Wave Optics. Short course presented at the Society of Photo-Optical Instrumentation Engineers, Cambridge, 1985. KTA values are from ref 30.

Pockels effect allows one to alter this coupling by applying a voltage to the crystal, changing the refractive index of the waveguide. Waveguide modulators include the phase modulator, which shifts the optical phase in a wave guide channel by altering an applied voltage, and the Mach-Zehnder intensity modulator. In the latter, the incoming signal is split between two waveguide "arms", where a differential in applied voltage induces a relative phase shift between the optical paths, resulting in either constructive or destructive interference upon recombination of two beams.[35]

Electrooptic r_{ijk} coefficients have been measured for KTP to determine their suitability for electrooptic modulator applications. A common figure of merit for guided-wave electrooptic modulators is n^3r/ϵ_{eff}, which relates to a bandwidth/driving voltage ratio. KTP is found to have a value of 17.3 pm/V for n^3r/ϵ_{eff}, which substantially exceeds values for other materials under consideration for integrated optic applications, such as $LiNbO_3$ and GaAs (Table IV).[29] Recently, r_{ijk} values have been measured for the KTP isostructure $KTiOAsO_4$ (KTA) as well (Table IV), and it is found that KTA's figures of merit for both bulk and waveguide electrooptic modulators substantially exceed KTP's.[30]

Waveguides are made in KTP by sputtering an Al or Au mask onto the (001) surface of the crystal, removing a narrow strip of this film, and exposing the surface to a nitrate melt containing alkali-metal ions more refractive than K^+ (e.g., Rb^+, Cs^+, Tl^+) between 350 and 450 °C.[13] Ion exchange between the surface and the melt occurs, creating a narrow channel of increased refractive index. Due to the anisotropy of the ionic mobility, the ions diffuse preferentially along the c direction; lateral diffusion out of the wave guide is minimal. This contrasts with Ti:$LiNbO_3$ waveguides prepared by high-temperature (1000 °C) Ti in-diffusion,[36] in which the region of Ti doping tends to stray outside the wave guide boundary. Additionally, once the larger ions are exchanged into the surface, their diminished mobility prevents further diffusion to the interior, giving a sharp depth profile to the wave guide. Guided-wave devices that have been fabricated on KTP substrates include single-channel phase modulators[29] and Mach-Zehnder interferometers.[37]

5. Synthesis. KTP melts incongruently at approximately 1170 °C.[38] This prohibits the use of melt–growth techniques such as the Czochralski method, which is applicable to such materials as $LiNbO_3$ and $BaTaO_3$. Crystals of KTP must therefore be grown from an aqueous flux (hydrothermal method), or a nonaqueous melt (flux method). KTP powder is also accessible from the simpler solid-state and gel growth techniques, but these methods are inappropriate for single-crystal growth, as they do not yield crystallite sizes larger than several micrometers.

The goal of research in KTP synthesis is 2-fold: both larger and less expensive crystals are required if KTP is to dominate the SHG field and to compete successfully with $LiNbO_3$ and other ferroelectrics as materials for electrooptic modulators. The current price of optical grade KTP crystals 4–5 mm on edge, cut, polished, coated, oriented for YAG SHG, and sufficiently large for high-power Q-switched lasers, is on the order of $300 000/oz.[39]

The technique Airtron employs to grow KTP commercially is the hydrothermal method, in which TiO_2 or $KTiOPO_4$ nutrient dissolves in an aqueous KH_2PO_4 flux at 600 °C and 30 000 psi. The reaction is carried out inside a noble-metal can, which is welded shut prior to being immersed in a steel autoclave. The can prevents the hot phosphate solution from contacting and corroding the steel walls of the autoclave, which would result in contamination of the growing KTP crystals. Baffles separate the nutrient from the growth region, where seed crystals are suspended from a noble-metal tree by gold wires (Figure 6). After rapidly heating to 600 °C, the system is held at constant temperature. A temperature gradient is established, and as the hot nutrient solution is transported to the cooler end of the vessel, $KTiOPO_4$ is precipitated onto the seeds. Heating is continued over 5–6 weeks, at which time the autoclave is quenched.[40]

Other workers have investigated the hydrothermal phase space of KTP to determine if suitable crystals can be grown at lower temperatures. This would allow lower priced low-carbon steel autoclaves to be used, which would then be furnished with a noble-metal liner and seals, eliminating the need for a sealed tube. Laudise et al.[41] report that with use of a more basic flux solution of K_2HPO_4 at 400 °C, good quality crystals grow at the rate of approximately 0.07–0.14 mm/day. Similar results are reported by Jia et al. for growth of KTP in solutions containing KF as a mineralizer.[42] For a given temperature between 370 and 420 °C, solubility was enhanced as the F^- concentration increased from 1.0 to 4.0 M. These results suggest the potential of improved production of hydrothermally grown KTP at reduced cost.

Because it does not entail the expense of an autoclave, flux growth of KTP has been investigated as an alternate route to large single crystals. In this procedure, crystals are precipitated from a flux of approximate composition $K_6P_4O_{13}$ at temperatures between 1000 and 800 °C. After the run, the system is quenched and the remaining flux is dissolved away in hot water. This method is disadvantaged by the problem of greatly increased viscosity compared with hydrothermal fluxes, caused by dehydration and oligomerization of the phosphate to form KPO_3 glasses. This increased viscosity often results in supersaturation and flux inclusions. Jacco et al.[38] reported the growth of crystals up to 15 × 15 × 5 mm in size by seeding a melt in a rotating platinum crucible equipped with a cooling finger. A typical temperature profile consists of

(36) Becker, R. A. *Mater. Res. Soc. Bull.* **1988**, *13*(6), 21.
(37) Laubacher, D. B.; Guerra, V. L.; Chouinard, M. P.; Liou, J.-Y.; Wyat, P. H. *Proc. SPIE—Int. Soc. Opt. Eng.* **1988**, *993*, 80.
(38) Jacco, J. C.; Loiacono, G. M.; Jaso, M.; Mizell, G.; Greenberg, B. *J. Cryst. Growth* **1984**, *70*, 484.
(39) Belt, R. F., personal correspondence.
(40) Bierlein, J. D.; Gier, T. E. U.S. Patent 3,949,323.
(41) Laudise, R. A.; Cava, R. J.; Caporaso, A. J. *J. Cryst. Growth* **1986**, *74*, 275.
(42) Jia, S.-Q.; J.; Jiang, P.-Z.; Niu, H.-D.; Li, D.-Z.; Fan, X.-H. *J. Cryst. Growth* **1986**, *79*, 970.

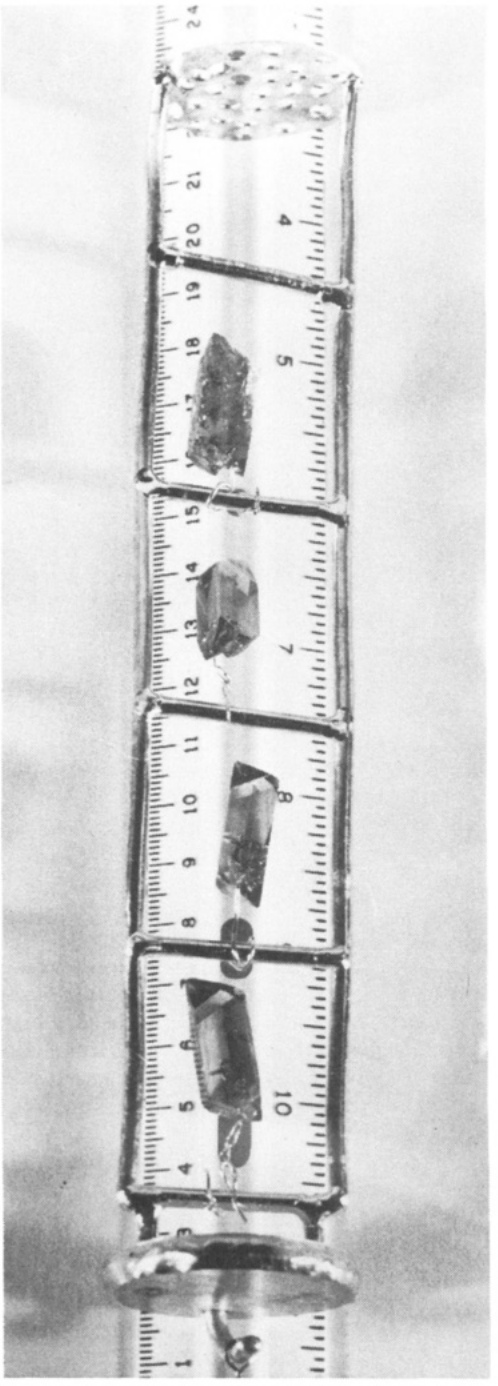

Figure 6. Hydrothermally grown KTP crystals, still suspended from rack by Au wires. The perforated baffle at the bottom of the rack separates the growing crystals from the nutrient. Photo courtesy of Du Pont.

cooling from 1020 to 960 °C at a rate of 0.5 °C/h, by using 170 L/h of cooling air. They have also reported growth of good-quality crystals up to 5 × 7 × 12 mm in size via gradient transport.

To reliably obtain better quality material from the phosphate fluxes, several additives have been tried in attempts to break the P–O–P oligomer linkages, thereby reducing the viscosity of the solution. One successful example is reported by Ballman et al.,[43] where tungsten trioxide was used along with K_2HPO_4 and TiO_2 to give spontaneously nucleated crystals of approximately 1 cm^3 in volume. Ballman et al. note that in addition to giving a "very fluid, non-glass-forming melt", the incorporation of tungstate results in a solubility vs temperature curve of shallow slope, resulting in a low degree of supersaturation. For a run where the ratio of flux to nutrient was given as $4K_2HPO_4{\cdot}2TiO_2{\cdot}3WO_3$, cooling was initiated from 1000 °C, with a typical rate of 1 °C/h. Other flux additives were tried by Jacco et al.; these included B_2O_3, CaO, PbF_2, V_2O_5, KF, and PbO. Of these, only PbF_2 was deemed successful. However, crystals grown from such a flux contained significant amounts of Pb, the effect of which on SHG performance has not been reported.[38]

The addition of potassium halides to the phosphate flux enhances the solubility of KTP. This phenomenon is responsible for an unusual variation on the flux growth method developed by Marnier[44] in which KF, KCl, or KBr is added to the standard TiO_2:phosphate flux, which is heated continuously at a temperature between 650 and 1100 °C. The potassium halides slowly volatilize from the melt, reducing the solubility of KTP, causing spontaneous nucleation of crystals. After crystallization is finished, the crystals and flux are slow cooled to room temperature to prevent thermal shock, and the flux is dissolved in water.

As was previously mentioned, KTP powder is accessible from a solid-state route. Here, TiO_2 is reacted directly with K_2HPO_4 by sintering stoichiometric quantities of each in a Pt or Al_2O_3 crucible at 950 °C overnight. The resulting white powder consists of irregular crystals of approximately 1-μm diameter. While this material is obviously of little utility for device applications, this technique has proven valuable in the synthesis of KTP derivatives where stoichiometric control is required.[45]

KTP powder may also be made by heating a Ti-containing hydrogel in the presence of excess potassium phosphates.[17] In this procedure, $TiCl_4$ is mixed with water to give a clear solution that is 1.82 F in $TiCl_4$. This is then added to a 10 M solution of K_2HPO_4 in water such that the PO_4:Ti ratio is 6:1. The resulting gel is shaken vigorously and autoclaved at autogenous pressure at 200 °C for 5 days. The resulting powder has an average crystallite size of approximately 2–3 μm, although individual particle sizes may exceed 20 μm. If TiO_2 (anatase) is substituted for the "$TiCl_4$" solution, the resulting product will contain residual TiO_2. KTP can be made easily, inexpensively, and in large quantity via this technique and, while unsuitable for harmonic generation and electrooptic applications, is useful as a nutrient for KTP crystal growth, for investigating chemical properties such as ion exchange, and in the synthesis of KTP isomorphs.

As noted above in the discussion on conductivity and shown by the lattice constant variation in Table I, it should be emphasized that the properties of KTP depend on the route by which it is synthesized. Ballman et al. point out that the KTP grown in tungstate flux deviates from the values quoted for KTP grown hydrothermally at Airtron mostly in the *a* dimension, which is longer than that of Airtron KTP by 0.04 Å or 0.3%, but decline to state whether the lower pressure or the presence of tungsten in the flux is responsible. The principal indexes of refraction also differ from those seen in hydrothermally grown KTP, which in turn is probably responsible for the small difference seen between the two materials in the phase-match angle at 1.064 μm.[43] Another obvious difference between flux grown and hydrothermally grown KTP is in their IR spectra. Hydrothermally grown KTP crystals generally show one or more absorption bands between 3550 and 3600

(43) Ballman, A. A.; Brown, H.; Olson, D. H.; Rice, C. E. *J. Cryst. Growth* **1986**, *75*, 390.

(44) Marnier, G. U.S. Patent 4,746,396.

(45) Phillips, M. L. F.; Harrison, W. T. A.; Gier, T. E.; Stucky, G. D. *Proc. SPIE—Int. Soc. Opt. Eng.*, in press.

Table V. Comparison of the SHG Properties of Several Inorganic Materials[a]

	phase-matchable wavelength, μm	d^2/n^3 (Re:KDP)	damage threshold, GW/cm²	Δθ, mrad cm	walkoff, mrad	Δλ, nm cm	ΔT, °C cm
$KTiOPO_4$	1.0–2.5	62	1–10	26/70	5	2	30
β-BaB_2O_4	0.4–3.3	13	1–10	1	60	4.5	37
$KNbO_3$	0.4–5	270	0.35	45	0	0.05	0.3
$LiNbO_3$	0.4–5	23	0.05	5–25	9–0	0.6	0.6
$LiIO_3$	0.3–5.5	40	0.5	0.8	75	1.4	50
KH_2PO_4	0.2–1.5	1	0.2–10	3–6	23	50	6–25

[a] From: Bierlein, J. D. Structure/Property Relationships in Optical Materials. Extended Abstracts, *MRS Proc. Symp. J.*, Fall 1987; Eimerl, D., Ballman, A. A., Lowe, C. K., Eds.; American Institute of Physics: New York.

cm^{-1} due to the presence of OH^- moiety. These bands are much less intense in flux-grown crystals, and the absorptions occur at different wavelengths, indicating that OH^- is sparser and in a different chemical environment in the flux-grown material than in KTP made hydrothermally.[46] The effects of these OH^- inclusions on device performance, if any, are not yet well characterized.

6. KTP Summary. Potassium titanyl phosphate is one of the most promising nonlinear optic materials known. The high nonlinear optical coefficient, high optical damage threshold, low threshold power, and low phase-matching sensitivity[23] make KTP the premier material used for second harmonic generation of the 1.064-μm YAG laser (Table V). Recent studies have also shown that KTP is optimum for intracavity sum frequency mixing of the 0.809-μm pump radiation and the 1.064-μm YAG frequency over a very wide range of temperatures (−50 to 300 °C).[12] In addition, large, high-quality single crystals can be prepared with the appropriate chemical and mechanical stability, to make excellent wave guides and electrooptic modulators.

Along with its exceptional optical properties, KTP has two structural features that suggest that it might provide the basis for developing a quantitative and predictive understanding of second-order wave-mixing phenomena at the atomic level. Specifically, these are (1) an open structural framework that permits the use of the host/guest relationships of inclusion chemistry to selectively modify electrooptic behavior and (2) the presence of two formula units/asymmetric unit of the unit cell, with all atoms in general positions of the acentric space group. With these attributes it should be possible to develop a structural field with an excellent opportunity to fine-tune electrooptic properties by displacive, inclusion, and substitution chemistry.

The problem is not trivial. The space-group symmetry of KTP, $Pna2_1$, results in five independent observable bulk susceptibility coefficients. The historical[47] and still commonly used assumption[48] is that since one is dealing with a scattering phenomena that perturbs only the electrons in the ground state, localized bonding units are all that need to be considered. In this localized model, the macroscopic NLO susceptibility (e.g., SHG coefficient $\chi^{(2)}_{ijk}$) can be expressed as the geometric superposition of the microscopic second-order susceptibility, β, of each bond. The second-order bulk susceptibility coefficient $\chi^{(2)}$ in eq 4 is related to the second-order electron (bond) polarizability tensor, β, in eq 3 by

$$\chi^{(2)}_{ijk} = (2/V) \sum_{i,m,n} a_{il} a_{jm} a_{km} \beta_{lmn} \qquad (6)$$

Table VI. Nonlinear Polarizabilities of Metal–Oxide Bonds[49]

B → O	$\beta_{\parallel}(\sigma)$	$\beta_{\perp}(\sigma)$	compd
Be → O	−3.08	−1.04	BeO
Zn → O	−12.4	−3.1	ZnO
S → O	7.0 (1)	2.1 (.3)	$LiKSO_4$
Cl → O	7.05	2.5	$NaClO_3$
N → O	7.3	3.0	$NaNO_2$
P → O	10.4	2.95	KH_2PO_4
Br → O	14.2	4.64	$NaBrO_3$
I → O	34.5 (1.6)	9.65 (.4)	$LiIO_3$
Ta → O	51 (1)	4.7 (1)	$LiTaO_3$
Nb → O	82 (7)	12 (3)	$LiNbO_3$
Ti → O	212	16	$BaTiO_3$

where a values are direction cosines relating the bond coordinates to crystal coordinates. For KTP the bond polarizability coefficients, β_{lmn} in eq 6, are defined by the structural and electronic properties of the 37 different oxygen atom bonds to Ti(1) (six), Ti(2) (six), P(1) (four), P(2) (four), K(1) (eight), and K(2) (nine). With this relatively simple localized bond parameter model and only the KTP structure, a large number of approximations obviously must be made to correlate bond properties to electrooptic behavior. *Currently all NLO models that might be used for structures with large distortions and structures as complicated as KTP have severe predictive limitations because of the problem of matching the number of model and observable parameters.* For this reason, studies of the functional dependence of β on charge distribution and bond length in an isostructural series such as that described within this review provides a particularly important basis for understanding nonlinear optic processes. A second approach is to examine the nonlinear optic response as a function of induced atomic displacements within a given structure. The following discussion reviews some aspects of both of these approaches.

4. Bonds and NLO Properties

Bergman and Crane[49] used the above bond parameter approach to carry out a systematic decomposition of the bulk nonlinear coefficients in terms of bond polarizabilities (β's) for oxide systems (not necessarily isostructural) of the form ABO_x (A = Li, Na, Ba, etc.; B = Nb, Ti, I, etc.) using the approximation that the point symmetry of the chemical bond can be approximated by C_∞. Assuming no dispersion, each bond polarization tensor is then reduced to two components, $\beta_{\perp}$ and $\beta_{\parallel}$, where the directions refer to bond axes. For cases where there are lone-pair electrons on the B atom as in IO_3^-, the value of β_{LP} is assumed to be $\approx\beta_{B\text{-}O}$. AO β's are neglected. The results of this analysis are shown in Table VI. This *bond parameter* model confirms that Ti–O, Nb–O, and I–O bonds are all highly polarizable (Table VI). Bergman and Crane rationalized the qualitative behavior of the observed values by a mi-

(46) Theis, W. M.; Norris, G. B.; Porter, M. D. *Appl. Phys. Lett.* **1985**, *46*, 1033.
(47) Robinson, F. N. H. *Bell Syst. Tech. J.* **1967**, *46*, 913.
(48) Chen, C. T.; Wu, B. C.; Jiang, A. D.; You, G. M. *Sci. Sin. (Engl. Ed.)* **1985**, *B28*, 235.
(49) Bergman, J. G.; Crane, G. R. *J. Solid State Chem.* **1975**, *12*, 172–175.

croscopic model that gives:

$$\beta = \alpha^3 p \quad (7)$$

where α is the linear polarizability for the bond and p is the bond dipole moment. This interesting relationship predicts a change in sign with ionicity: highly ionic compounds (e.g., early metals in low oxidation states) with the center of charge closest to the oxygen atom are expected to have negative β's, while positive β's are predicted for more covalent B–O bonds formed by high formal oxidation state atoms, including Ti. In any event, the first point of focus in defining the KTP NLO behavior is clearly the Ti–O bond.

The bond charge theory, developed by Levine,[50] describes the nonlinear hyperpolarizability of a bond in terms of a point *bond charge* residing in an asymmetric potential well.[20] The asymmetry is defined as a function of the electronegativity difference between the bonding atoms and the difference in their atomic radii. Levine's model invokes in more detail the idea of "dynamic covalency". In the harmonic oscillator model, the *low*-frequency linear susceptibility in crystals is inversely proportional to the bandgap, E_g. In an optical field, the bond charge is dynamically displaced, which results in a change of energy of the bandgap orbitals and E_g. This field dependence of the linear susceptibility gives rise to the second-order susceptibility β of each bond.

In addition, the bond charge model allows the nonlinearity of the bonds to vary with distance according to the relation

$$\beta = \beta_0 (d/d_0)^{\sigma_{NL}} \quad (8)$$

which is used to give the dependence of the nonlinear parameter, β, on bond length.[50] β_0 is the average value of the bond nonlinearity, d_0 is the average bond length, d is the actual bond length, and σ_{NL} can be calculated from observed second-order susceptibility coefficients. The nonlinearity of such systems as $LiNbO_3$, $Ba_2NaNb_5O_{15}$, and $LiTaO_3$, in which the metal atom resides in a nearly octahedral field, is thus accounted for by considering the unequal contributions of the short and long metal–oxygen bonds. The treatment of these systems is simplified by disregarding the highly ionic cation–oxygen bonds and neglecting $\beta_\perp$. This results in close agreement between calculated and observed Δ_{ijk} values for $LiNbO_3$, but the discrepancy is larger for more complex niobates such as $Ba_2NaNb_5O_{15}$.[51] Levine includes among several possible sources of this discrepancy contributions from cation–oxygen bonds and notes that the form of the dependence of β on bond length, a fortuitous consequence of the bond charge model, represents a "severe" test of the theory.[20]

Zumsteg et al. used the bond charge model to calculate the microscopic susceptibilities in the $K_{1-x}Rb_xTiOPO_4$ system and concluded that the difference in trans-Ti–O bond lengths is the major contributor to Δ_{ijk}, although the magnitude of the nonlinearity of this bond is highly variable depending upon how the ionicity is calculated. Neither the (K,Rb–O) nor the (P–O) bonds are expected to contribute significantly to the total susceptibility.[8] Hansen et al. have recently followed up on this treatment by using detailed electron density maps from X-ray diffraction studies to measure the valence electron density distribution in KTP.[52] Again neglecting K–O and P–O contributions, the data define the Ti=O titanyl bond as being responsible for the large electrooptic coefficients in KTP, although the theoretical Δ's were found to be substantially less than those observed experimentally. Furthermore, Hansen et al. describe the long Ti–O bonds trans to the titanyl bonds as being unimportant in defining the NLO coefficients.

The conclusion presented by these models is that the variation in trans-Ti–O bond lengths is responsible for the large bond polarizability and value of β. A difficult problem in all of the models and implied by the qualitative description of Crane and Bergman is the quantitative dependence of the second-order NLO response on bond length. Ti–O bond lengths are notoriously variable, ranging from $\approx$1.7 to 2.3 Å. In fact, for BO_6 octahedra in ferroelectric crystals, the two trans bonds which are parallel to the polarization direction can have contributions that differ in *both* magnitude and sign.[53] Therefore, the results obtained for the bond charge model (eq 8) unfortunately give variations in the values of σ_{NL} excessively large to be physically meaningful or predictive.[53,54] It should be emphasized that the above models were derived from consideration of simple structures, and clearly a more generalized model is needed for predicting the NLO properties of new materials.

Recognizing the limitations of the bond order and bond charge models, Chen has proposed a more extended model that also begins with the hypothesis that the NLO susceptibility in crystals is a localized effect of the incident light on the electrons in certain clusters of orbitals.[55] Because electrooptic and nonlinear optic effects arise from the perturbation of electrons by the incident radiation, with the electrons still being in their ground state, short-range forces play a principal and decisive role in determining the resulting motion of the electrons. The region of the localized motion of the electrons is defined by the *anionic group* model to be the (MO_6) oxygen atom group for six-coordinate metal atoms, the (PO_4) unit for phosphates, (IO_3) for iodates, etc. The overall SHG then is determined by the geometrical superposition of these groups and has little to do with the cation. Second, the microscopic SHG coefficients of the anionic groups can be calculated by using the localized molecular orbital wave functions of the groups with second-order perturbation theory.

It is perhaps useful at this point to very briefly outline this molecular orbital approach to understanding nonlinear optic behavior.[56] Since the perturbation to the electron density in our crystal is the time-dependent electric field, $E(t)$ of the light, we must start with the time-dependent Schrödinger equation:

$$H\Psi = i\hbar \frac{\partial \Psi}{\partial t} \quad (9)$$

where

$$H = H_0 + H' = H_0 - e\mathbf{E}\cdot\mathbf{r} \quad (10)$$

The perturbation $H' = -e\mathbf{E}\cdot\mathbf{r}$ is the interaction of the applied field with the molecule in the electric dipole ap-

(50) Levine, B. F. *Phys. Rev. B* **1974**, *10*, 1655.
(51) The use of Miller's Δ is preferred here over d_{ijk}, as it is less sensitive to variations in linear polarizability. See: Miller, R. C. *Appl. Phys. Lett.* **1964**, *5*, 17–19.
(52) Hansen, N. K.; Protas, J.; Marnier, G. *C. R. Acad. Sci. Paris Ser. II*, **1988**, *307*, 475–8.
(53) Levine, B. F. *Phys. Rev. B* **1976**, *13*, 5102.
(54) Fuji, Y.; Sakudo, T. *Phys. Rev. B* **1976**, *13*, 1161.
(55) Chen, C.-T. *Ann. Rev. Mater. Sci.* **1986**, *16*, 203–243, and references therein.
(56) For a comprehensive description of current throughts in this area, the reader is referred to articles by: Zyss, J.; Chemla, D. S. (p 23); and Pugh, D.; Morley, J. O. (p 193). In Nonlinear Optical Properties of Organic Molecules and Crystals. *Quantum Electronics—Principles and Applications Series*; Liao, P. F., Kelley, P., Eds.; Academic Press: New York, 1987; Vol. 1. A detailed description of Chen's approach for inorganics is described in the bibliography of ref 53 of this review.

proximation. **r** is the general dipole moment operator and is the sum of the individual dipole moments for all the electrons. Following the textbook procedure for evaluating time-dependent perturbations,[57] the solutions correct to third order are given by

$$\Psi_m(\mathbf{r},t) = \sum C_{mn}(t)\ \Psi^{(0)}{}_n(\mathbf{r},t) \qquad (11)$$

There are several important aspects of the formalism that are helpful in understanding NLO behavior. The $\Psi_m(\mathbf{r},t)$ eigenfunctions describe the new electronic state of our perturbed system in terms of linear combinations of the original $\Psi^{(0)}{}_m(\mathbf{r},t)$ electronic states. Importantly, as time proceeds, the new electronic state is described by different ground-state mixtures. This "dynamic covalency" can be coupled with crystal anisotropies or even phonon-induced structural displacements to give large electron polarizabilities. For example, suppose that the combination of original states includes the ground state and an excited state that has a large charge reorganization with a correspondingly large excited-state dipole. We have in effect greatly increased the anharmonicity of our potential well and β, the second-order polarizability.

The polarization and distortion of the electrons can thus be described by mixing other states of the system into the one of interest. It has been decided to describe this by saying that the perturbation induces transitions to these other states. Obviously they are not real transitions, but diagramatically they are visualized as *virtual* transitions. The NLO behavior is then viewed in terms of the ground- and excited-state dipole moments, e.g., $\langle g|\mathbf{r}|g\rangle$ or $\langle e|\mathbf{r}|e\rangle$, and transition moments, e.g., $\langle g|\mathbf{r}|e\rangle$ or $\langle e|\mathbf{r}|e'\rangle$, where g is an initial ground-state wave function and e,e' are the virtual-state (unperturbed excited state) wave functions. The perturbation mixing of ground and excited states is then described by summing over the appropriate dipole and transition moments, i.e., a "sum over states". This "sum over states" approach has been extensively used in the description of organic NLO properties.[58]

Abstracting the localized moieties described above from the extended inorganic structures, Chen then calculates the localized electron orbitals ($\Psi^{(0)}{}_n$ in eq 11) in the anionic groups using CNDO approximations. These eigenfunctions are used to determine the single or two-center dipole transition matrix, the diagonal elements of which give the individual state dipole moments. Products of these moments divided by the appropriate combination of virtual-state transition energies gives the NLO coefficients for the anionic group. The last step is to use eq 6 to relate the resulting anionic group polarizabilities to the macroscopic SHG $\chi^{(2)}$ values of eq 4.

Relatively good agreement has been reported by Chen for a variety of metal oxide perovskite and tungsten bronze type crystals, β-BaB_2O_4, iodates, phosphates, and nitrites. The agreement for highly distorted anion groups such as those found in KTP is less desirable. For the purposes of this review several conclusions drawn from this model will be noted: (1), the cation (K^+ in KTP) plays little or no role in SHG behavior, (2) the larger the deformation of (MO_6) coordination octahedra, the larger the microscopic second-order susceptibility will be, and (3) when two oxygen octahedra are not isolated, e.g., when two adjacent

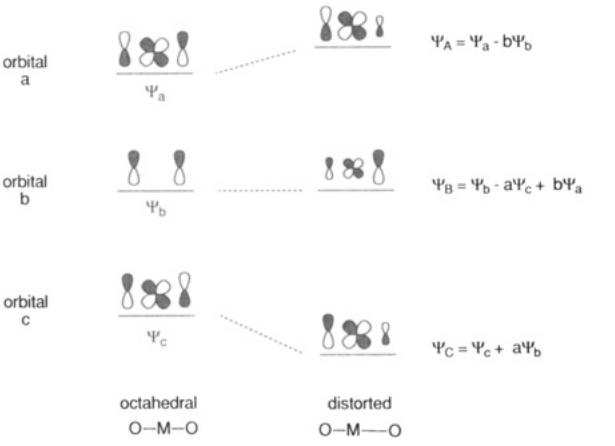

Figure 7. Mixing of M–O orbitals on distortion from octahedral symmetry and consequent stabilization of resulting ground state.

octahedra share one oxygen atom, the SHG coefficient will depend entirely on (MO_6) octahedra and their mode of distortion.

More recently, Burdett et al. have considered the role of the extended framework in determining M–O bond alternation[59] in early-transition-metal chemistry. This has been applied to a study of the relationship of electron induced M–O bond alternation to the observed NLO behavior of members of the KTP structural field.[60] The bond alternation found in perovskites, linear-chain compounds such as KTP, and several cyclic systems may be understood in terms of a second-order Jahn–Teller effect which couples the largely oxygen nonbonding levels at the top of the oxygen p band with the metal–oxygen antibonding levels of the metal d band.[61]

In a local sense this can be viewed as shown in Figure 7, which shows the relevant orbitals of an octahedral MO_6 unit and how they mix as the geometry changes. Oxygen $p\pi$ and metal $d\pi$ orbitals mix to form bonding, nonbonding, and antibonding orbitals, respectively, of g, u, and g symmetry with respect to inversion. Simple perturbation theory allows access to the mixing of g and u orbitals during an asymmetric distortion. Both the interaction energies and the orbital mixing coefficients a and b depend upon the size of the energy gaps between the relevant orbitals at the octahedral geometry and the overlap integrals between the orbitals. The magnitude of the mixing coefficients both at the octahedral geometry and on distortion are readily extracted from the results of a simple extended Hückel calculation. The resulting stabilization is competing with the destabilization associated with other occupied orbitals, i.e., Coulomb repulsion effects, and the compromise between these two determines the actual magnitude of the distortion.

Importantly the orbitals of Figure 7 are intimately connected with the nonlinear optical properties of the system. Figure 8 shows how the β_{zzz} component of the polarizability along the O–Ti–O axis progresses from an

(57) For a start, see: Atkins, P. W. *Molecular Quantum Mechanics, An Introduction to Quantum Chemistry*; Clarendon Press: Oxford, 1970; Vol. 1.

(58) The tabulation of the second- and third-order coefficients in terms of the virtual-state transition energies and the dipole operator matrix elements has been explicitly given by Ward (Ward, J. F. *Rev. Mod. Phys.* **1965**, *37*, 1) and by Orr and Ward (Orr, J. B.; Ward, J. F. *Mol. Phys.* **1971**, *20*, 513).

(59) Burdett, J. K.; Hughbanks, T. *Inorg. Chem.* **1985**, *24*, 1741. Burdett, J. K. *Inorg. Chem.* **1985**, *24*, 2244.

(60) Phillips, M. L. F.; Harrison, W. T. A.; Stucky, G. D.; Kulkarni, G. V.; Burdett, J. K. *J. Am. Chem. Soc.* submitted for publication.

(61) An interesting aspect of metal oxide bond instabilities has been pointed out by Bilz, Schwarz and co-workers Bussman, A.; Bilz, H.; Roenspiess, R.; Schwarz, K. *Ferroelectrics* **1980**, *25*, 343). The O^{2-} ion is configurationally unstable as a free ion but can be stabilized by long-range crystalline Coulomb effects. This instability coupled with covalency and crystal anisotropy gives linear polarizabilities which vary as r^{12} (r = M–O bond length) in spinels and r^6 in ferrolectric perovskites. The results illustrate the inherent danger of neglecting long-range band and phonon structure in predicting NLO behavior.

Table VII. Isomorphous Derivatives of KTP[a]

compd	SHG[64]	a, Å	b, Å	c, Å	synthetic route	ref
		(M,M')$TiOPO_4$ Compounds				
$KTiOPO_4$	6000	12.814	6.404	10.616	hydrothermal	8
$NaTiOPO_4$	160	12.615	6.281	10.585	ion exchange	45
$AgTiOPO_4$	5	12.524	6.263	10.530	ion exchange	17
$Ag_{0.85}K_{0.15}TiOPO_4$	7	12.534	6.294	10.524	ion exchange	17
$Ag_{0.5}K_{0.5}TiOPO_4$	130	12.552	6.333	10.602	ion exchange	17
$(NH_4)_{0.5}H_{0.5}TiOPO_4$	6	12.822	6.284	10.598	desorption	18
$(NH_4)_{0.5}K_{0.5}TiOPO_4$	1100	12.894	6.442	10.580	hydrothermal	62
$Rb_{0.5}K_{0.5}TiOPO_4$	6000	12.916	6.443	10.546	hydrothermal	62
$TlTiOPO_4$	6000	12.983	6.490	10.578	flux	15
$(NH_4)_5(H_3O)_5TiOPO_4$	700	12.915	6.494	10.589	desorption/resorption	18
NH_4TiOPO_4	1100	12.915	6.492	10.598	hydrothermal	18
$RbTiOPO_4$	6000	12.971	6.492	10.577	flux	15
		(M,M')TiO(P,As)O_4 Compounds				
$KTiOAsO_4$	6000	13.103	6.558	10.746	flux	65
$KTiO(PO_4)_{0.5}(AsO_4)_{0.5}$	6000	12.950	6.478	10.677	flux	62
$TlTiOAsO_4$	6000	13.208	6.686	10.724	flux	65
$(NH_4)_{0.5}K_{0.5}TiOAsO_4$	100	13.157	6.592	10.809	ion exchange	45
$NH_4TiOAsO_4$	100	13.212	6.678	10.793	gel growth	45
$RbTiOAsO_4$	6000	13.242	6.689	10.755	flux	65
$Cs_{0.5}K_{0.5}TiOAsO_4$	6700	13.311	6.662	10.800	solid state	62
		Tetravalent Main-Group and Transition-Metal KTP Derivatives				
$NaGeOPO_4$	4	12.326	6.094	10.117	solid state	17
$KGeOPO_4$	3.3	12.602	6.302	10.006	gel growth	71
$KVOPO_4$	N/A	12.717	6.382	10.513	hydrothermal	17
$KGeOAsO_4$	0.03	12.85	6.54	10.08	solid state	62
$KSnOPO_4$	0.0	13.146	6.528	10.727	solid state	72
$RbSnOPO_4$	0.0	13.332	6.618	10.720	solid state	17
$KSnOAsO_4$	0.53	13.417	6.687	10.977	gel growth	62
$RbZrOAsO_4$	3	13.735	6.908	11.440	flux	62
$NH_4ZrOAsO_4$	1	13.681	6.886	11.583	ion exchange	62
$CsZrOAsO_4$	2	13.796	6.982	11.23	solid state	62
		Mixed-Valent KTP isostructures				
$KGaPO_4F_{0.7}(OH)_{0.3}$	0.72	12.715	6.304	10.433	hydrothermal	17
$KTi_{0.5}Ga_{0.5}O_{0.5}PO_4F_{0.35}(OH)_{0.15}$	200	12.802	6.352	10.503	gel growth	45
$KFePO_4F$	2.66	12.854	6.372	10.670	gel growth	73
$KGa_{0.5}Nb_{0.5}OPO_4$	1.0	12.94	6.47	10.62	solid state	62
$RbGa_{0.5}Nb_{0.5}OPO_4$	1.0	13.107	6.490	10.490	solid state	62
$KFe_{0.5}Nb_{0.5}OPO_4$	2.7	12.960	6.466	10.696	hydrothermal	17
$KGaAsO_4F$	0.02	13.04	6.47	10.61	gel growth	62
$KMg_{0.33}Nb_{0.67}OPO_4$	0.0	13.079	6.516	10.929	solid state	62
$KMn_{0.5}Nb_{0.5}OPO_4$	0.0	13.122	6.569	10.911	solid state	62
$KGa_{0.5}Nb_{0.5}OAsO_4$	1.0	13.24	6.62	10.80	solid state	62
$KFeAsO_4F$	1.0	13.21	6.54	11.15	gel growth	62
$RbGa_{0.5}Nb_{0.5}OAsO_4$	5.5	13.403	6.71	10.74	solid state	62

[a] Typical estimated standard deviations in the above lattice parameters are 0.004 Å for the *a* and *c* values and 0.002 Å for *b* values. Cell dimensions reported to two decimal places should be considered accurate to ±2 in the last place for *a* and *c* and ±1 in the last place for *b*.

Table VIII. Trans Ti–O Bond Distances (Angstroms) in KTP Isostructures

compd	Ti(1)–O(1)	Ti(1)–O(9)	Ti(1)–O(10)	Δ(1–10)	Ti(2)–O(9)	Ti(2)–O(10)	Δ(9–10)
$KTiOPO_4$	2.161 (4)	1.993 (4)	1.718 (4)	0.443 (6)	1.738 (4)	2.101 (4)	0.363 (6)
NH_4TiOPO_4	2.148 (4)	1.967 (3)	1.717 (3)	0.438 (5)	1.742 (4)	2.096 (4)	0.354 (6)
$TlTiOPO_4$	2.154 (5)	1.961 (5)	1.725 (5)	0.429 (7)	1.747 (5)	2.076 (5)	0.329 (7)
$RbTiOPO_4$	2.148 (5)	1.967 (4)	1.722 (5)	0.426 (7)	1.750 (5)	2.094 (5)	0.344 (7)
$AgTiOPO_4$	2.228 (11)	1.998 (11)	1.709 (11)	0.519 (16)	1.783 (12)	2.073 (11)	0.290 (16)
β-$NaTiOPO_4$	2.229 (6)	2.007 (6)	1.714 (6)	0.515 (8)	1.755 (6)	2.102 (6)	0.347 (8)
$(NH_4)_{0.5}H_{0.5}TiOPO_4$	1.947 (4)	2.012 (4)	1.901 (4)	0.046 (6)	2.114 (5)	1.764 (5)	−0.350 (7)
$NH_4H_3OTi_2(PO_5)_2$	2.15 (3)	2.04 (2)	1.70 (2)	0.45 (4)	1.79 (2)	2.04 (2)	0.25 (3)
$KTiOAsO_4$	2.138 (15)	1.957 (16)	1.735 (16)	0.403 (22)	1.770 (19)	2.097 (19)	0.327 (27)
$KTiO(P_{0.5}As_{0.5})O_4$	2.153 (7)	1.975 (8)	1.727 (7)	0.426 (11)	1.759 (8)	2.091 (8)	0.332 (11)
$K_{0.5}(NH_4)_{0.5}TiOAsO_4$	2.153 (11)	1.984 (11)	1.731 (11)	0.422 (16)	1.763 (11)	2.123 (11)	0.360 (16)
$KVOPO_4$	2.089 (7)	2.051 (7)	1.673 (8)	0.416 (11)	1.671 (8)	2.199 (8)	0.528 (11)
$KGaPO_4F_{0.7}(OH)_{0.3}$	1.914 (6)	1.996 (6)	1.941 (6)	−0.027 (8)	1.925 (5)	1.981 (6)	0.056 (8)
$TlTiOPO_4$ (650°)	2.054 (10)	1.823 (9)	1.823 (9)	0.231 (13)	1.901 (7)	1.901 (7)	0.000 (10)

undistorted structure with a given Ti–O distance (R_{av}). 2Δ′ (Δ in Table VIII) is the difference in the two trans-Ti–O distances, and R_{av} is the average of the two equilibrium Ti–O distances. Notice that the plot indicates a maximum in the hyperpolarizability along with a change of sign for large distortions. This result parallels that of Bergman and Crane, obtained via a very different model.

In the following discussion the predictions of the above models are compared with the experimental nonlinear optic properties of selected members of the KTP structural field.

5. KTP Structure Field

We will approach the compositional phase space of this

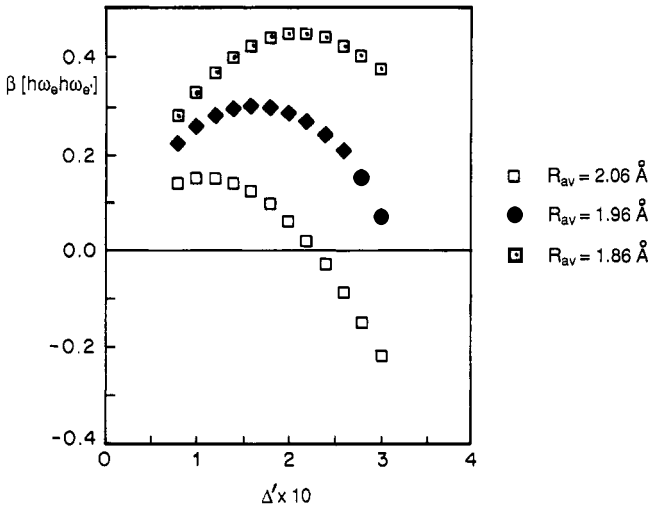

Figure 8. Dependence of nonlinear polarizability on distortion from octahedral symmetry. Δ' used here and in text is related to Δ in Table VIII by $\Delta' = \Delta/2$.

field in terms of the inclusion chemistry of KTP. This has practical significance both in terms of the synthesis of otherwise inaccessible phases and for electrooptic applications. The host framework is defined by the Ti=O helix and the phosphate groups that fill out the six-coordination sites at the titanium atoms to tie the helixes together. The cations (K^+) are the guests, which as noted above can have relatively high ionic conductivities.

The unit-cell volumes of the KTP structural analogues synthesized in our laboratory vary from 759.9 Å^3 for $NaGeOPO_4$ to 1095.8 Å^3 for $CsZrOAsO_4$, *an increase of 44%* (Table VII). Modifications can be made to the host structure by substitution at the titanium, phosphorus, or oxygen atom sites. Guest exchange can be carried out by substitution during synthesis, by ion-exchange, or in a few cases by small-molecule gaseous exchange. Specific examples include (1) F^- and OH^- chain bridging atoms in the KTP structure,[17] (2) mixed-metal (e.g., Fe^{3+}/Nb^{5+}) substituent for Ti^{4+},[17] (3) main-group members of the KTP structural family that have optical windows in the ultraviolet for possible higher order harmonic applications,[45] and (4) demonstration of the use of gas-phase absorption and desorption to switch or tune nonlinear optic properties in this family.[18] Table VII tells only part of the story since it follows that because these are inclusion materials with two formula units/unit cell, an incredibly large number of compositions can be made by using guest and host substitution. Also, as shown in two of the systems, $K_{1-x}(NH_4)_xTiOPO_4$ and $K_{1-x}(NH_4)_xTiOAsO_4$, this feature allows us to explore the role of selective versus disordered siting in defining SHG response.

1. Guest Phase Compositions. $MTiOPO_4$ compounds isomorphous with KTP, where M = Na^+, Tl^+, NH_4^+, or Rb^+, may be prepared directly, with complete substitution possible for Rb^+,[15] NH_4^+,[18] and Tl^+ [15] and partial substitution attainable with Na^+.[45] Due to the openness of the channels in which the cations reside, potassium ions may be exchanged out and replaced by other cations. Complete substitution by sodium and silver is attainable via this route, yielding the KTP isostructures β-$NaTiOPO_4$ (NaTP)[45] and β-$AgTiOPO_4$ (AgTP).[17] If arsenic replaces phosphorus on the tetrahedral site, the isostructure $KTiOAsO_4$ or KTA results. Rb^+, NH_4^+, and Tl^+ can still completely occupy the cation sites, but the compositional limits of ions at the extremes of size now favor the larger cations. For example, Cs^+ can attain 50% occupancy, but the maximum Ag^+ occupancy has been reduced to 50%. Arsenic can also partially replace phosphorous, and the complete range of solid solutions with the general formula $KTiO(PO_4)_{1-x}(AsO_4)_x$ is readily prepared (Table VII).[62]

2. Host Metal Ion Substitution Compositions. Other tetravalent transition-metal and main-group ions such as V(IV), Zr(IV), Ge(IV), and Sn(IV) may replace titanium on the six-coordinate sites, yielding KTP isostructures (Table VII). In the $MGeOPO_4$ series, the smaller size of the Ge ion allows Na^+ to easily replace K^+,[17] and unlike NaTP, $NaGeOPO_4$ may be synthesized directly. Similarly, replacing Ti with the larger Zr(IV) ion permits 100% occupancy on the cation sites by Cs^+. This is demonstrated in the compound $CsZrOAsO_4$, which has the largest unit cell volume of any of the KTP isostructures studied to date.[62] Vanadium can replace Ti to yield $KVOPO_4$, which, despite the difference in electronic configuration, is structurally very similar to KTP. The vanadium(IV) atom is a d^1 species, and the structure of KVP contains at 1.673 Å the shortest M–O distance found in the series. This very short distance ensures that the two π orbitals involved in this linkage are pushed to higher energy such that the lone electron lies in an orbital of δ symmetry with respect to the O–V–O axis. As far as the nonlinear properties are concerned it may be ignored, in first order at least, since these π and δ orbitals are orthogonal. The presence of the d electron on vanadium, however, causes $KVOPO_4$ to absorb visible light, and crystals of KVP therefore appear orange when viewed in transmission.[21] Several tetravalent metals have also been shown to partially replace Ti to yield solid solutions with the formulas $KTi_{1-x}Ge_xOPO_4$,[62] $KTi_{1-x}V_xOPO_4$,[21] and $KTi_{1-x}Sn_xOPO_4$;[63] these materials are isomorphous with KTP at any value of x.

Another method of balancing charge is by introducing a pentavalent ion, such as Nb(V), along with di- or trivalent ions onto the octahedral sites in the amount required to preserve overall neutrality. Some examples of these mixed III–V valent, II–V valent, and II–IV valent compounds are listed in Table VII.

3. Host Oxygen Atom Substitution Compositions. Divalent and trivalent cations may also replace Ti on the octahedral sites if fluoride and/or hydroxide are allowed to balance charge by replacing oxide on the sites bridging the six-coordinate positions. If Ti is replaced by Ga, for example, it is found that both F^- and OH^- are required for successful synthesis, and the result is a compound with the formula $KGaPO_4F_{0.7}(OH)_{0.3}$.[17] Partial Ti substitution is again possible, and the KTP structure results throughout the $KGa_xTi_{1-x}O_{1-x}PO_4(F_{0.7}(OH)_{0.3})_x$ series.[45] If divalent metals such as Mg replace Ti, 2 mol of fluoride or hydroxide per mol of divalent cation is required to balance charge. $K_2MgTi(PO_4)_2F_2$ is therefore the compositional limit of the magnesium-substituted series, and no end member containing only Mg can be prepared with the KTP structure.

4. Role of Host β_{MO} in SHG Response. As is evident from the results presented in Table VII, large SHG intensities are generally obtained only for members of the $MTiOPO_4$ and $MTiOAsO_4$ series, in agreement with the early observations of Bergman and Levine concerning the anomalous polarizability of the short Ti=O bond. In the main-group KTP isostructures that have been studied, the long–short metal–oxygen distance alternation seen in KTP

(62) Gier, T. E.; Harrison, W. T. A.; Phillips, M. L. F.; Stucky, G. D., unpublished data.
(63) Jarman, R. H.; Grubb, S. G. *Proc. SPIE—Int. Soc. Opt. Eng.* **1988**, *968*, 108–111.

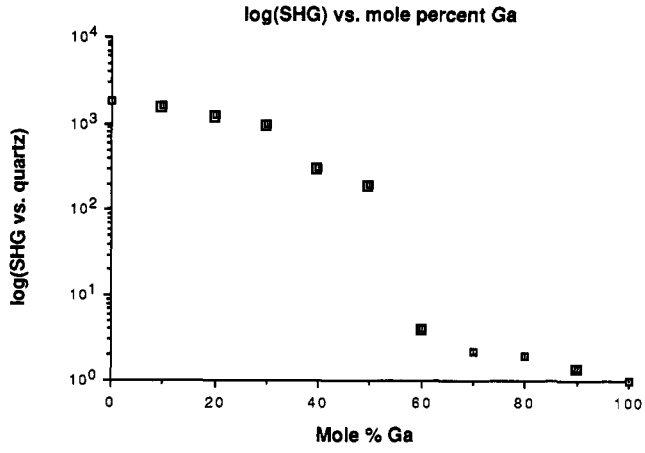

Figure 9. Compositional dependence of SHG intensity in the system $KGa_xTi_{1-x}O_{1-x}PO_4$ $(F_{0.7}(OH)_{0.3})_x$.

disappears. This is evident in the structural results obtained for single-crystal X-ray structure refinement of $KGaPO_4F_{0.7}(OH)_{0.3}$,[17] for example. The largest powder SHG intensity reported at this time for structural compositions containing no Ti is 10 times that of quartz, for the compound $KGa_{0.5}Ge_{0.5}O_{0.5}PO_4(F,OH)_{0.5}$[17] (Table VII).

A. $KGaPO_4F_{0.7}(OH)_{0.3}$.[17] This compound is made by reacting Ga_2O_3 with a stoichiometric excess of KH_2PO_4 and KF in water. At 200 °C and 15 bar this reaction yields a powder with a uniform crystallite size of approximately 3 μm. At 700 °C and 2.5 kbar, single crystals are obtained. The given stoichiometry, with its 2:1 F^-/OH^- ratio, appears to be fixed, and neither $KGaPO_4F$ nor $KGaPO_4OH$ have been prepared. If the F/Ga ratio in the starting material falls below 0.7, new, unidentified phases emerge. Attempts to obtain $KGaPO_4F$ using an anhydrous flux or a solid-state route similarly fail.

Single-crystal X-ray data from $KGaPO_4F_{0.7}(OH)_{0.3}$ reveal that the Ga(O,F) octahedra are much more regular than they are in KTP and that there are no longer any short metal–oxygen bonds (Table VIII). Since the powder SHG intensity[64] of this material is only on the order of that of quartz, we may postulate that the slight Ga–O bond-length differences and the Ga–O bond polarizability are insufficient to allow a nonlinear response of KTP's magnitude. Due to the similar scattering factors of fluorine and oxygen, it is not possible to tell from the X-ray data whether the F and O order themselves among the bridging positions between the Ga octahedra or if they instead occupy random positions in the chain. No hydrogen atoms, which would presumably be bonding to bridging oxygens, were found.

Ga may be partially included in the KTP host lattice to give a series of solid solutions with the general formula $KGa_xTi_{1-x}O_{1-x}PO_4(F_{0.7}(OH)_{0.3})_x$.[45] If the log of SHG intensity is plotted against the mole fraction of Ga for particles of similar size (Figure 9), we find that SHG intensity falls from nearly 2000 times that of quartz in KTP to 1 times that of quartz for $KGaPO_4F_{0.7}(OH)_{0.3}$. A distinct "break" or inflection point occurs between 50 and 60% Ga substitution and corresponds to a 50-fold drop in SHG intensity.

So far, the data support at least two possible explanations as to why the SHG intensity declines steeply as the 50 mol % boundary is crossed. One possibility is a phase transition may be occurring between a KTP-like phase with short metal–oxygen bonds on the Ti-rich side, and a $KGaPO_4F_{0.7}(OH)_{0.3}$-like phase on the Ga-rich side lacking any short metal–oxygen bonds. Another hypothesis suggests that there is selective siting between Ga and Ti for the octahedral sites and that incorporation of Ga onto either the cis or trans Ti position voids the contribution to the bulk susceptibility by the entire asymmetric unit. This theory is supported by the nearly linear decline in SHG intensity between 0 and 50% Ga, since every Ga atom added to the lattice would eliminate the microscopic nonlinearity of two octahedral sites.

In contrast with this material, the compound $KTiOAsO_4$ presents a case where minimal structure change is associated with a substantial augmentation in electrooptic and nonlinear optical coefficients.

B. Potassium Titanyl Arsenate (KTA). $KTiOAsO_4$ is accessible from any of the routes used to prepare KTP. Flux-grown crystals were used in the structure determination reported by El Brahimi and Durand[65] and in the measurement of its linear and nonlinear optical properties by Bierlein et al.[30] The crystallographic studies show that KTA is essentially isomorphous with KTP and that any structural differences not directly associated with the larger As atom are quite minor. The short Ti=O bonds in KTA are actually longer than they are in KTP, differing by 0.017 Å for Ti(1) and 0.032 Å for Ti(2); the difference in trans-Ti–O distances is also slightly reduced (Table VIII).

The data from Bierlein et al. show a significant enhancement of KTA's electrooptic and nonlinear optic coefficients versus those of KTP. The effective doubling coefficient d_{eff} for a type II interaction is 60% higher in KTA than in KTP. This cannot be accounted for by merely considering the increased linear polarizability due to substitution of As, as the refractive indexes of KTA are only about 3% higher than those of KTP (Table II). The electrooptic r_{ijk} terms are augmented as well (Table IV) with little change in dielectric constants, and KTA's figures of merit for both bulk and optical wave guide modulators are significantly greater than KTP's. Additionally, the ionic conductivity of KTA is about one-tenth that of KTP similarly grown from flux, although whether this is due to smaller defect concentration, obstruction of the channels parallel to [001] by the larger AsO_4 groups, or the increased basicity of the AsO_4 oxygen atoms (versus PO_4) is not yet clear. It is apparent from these data, though, that KTA presents itself as a feasible alternative to KTP and may even ultimately surpass KTP in terms of applicability.

In light of the previously discussed arguments defining the deformation of the TiO_6 octahedra and the short Ti=O bond in particular as the source of optical nonlinearity in KTP, it is surprising that KTA's electrooptic and nonlinear optic properties substantially exceed those of KTP. The 60% increase in the nonlinear optic response in KTA versus KTP in spite of the smaller deformation of the TiO_6 octahedra and the longer Ti=O bonds in the former is inconsistent with all of the above structural models unless $\beta_{As-O} \gg \beta_{P-O}$ by an amount not previously observed. This result alone emphasizes the point that consideration of the Ti=O or TiO_6 groups as isolated units in the KTP field can give only poor approximations to the experimental SHG values.

This question is currently being addressed by using the band structure approach described above.[59,60] Phosphorus is more electronegative than arsenic, and calculations show

(64) This and all powder SHG intensity data cited in this review were obtained in transmittance mode using equipment similar in configuration to the device described by: Dougherty, J. P.; Kurtz, S. K. *J. Appl. Crystallogr.* **1976**, *9*, 145. Unless otherwise noted, all SHG intensity values are referenced to those obtained on quartz samples.

(65) El Brahimi, M.; Durand, J. *Rev. Chim. Mineral.* **1986**, *23*, 146–153.

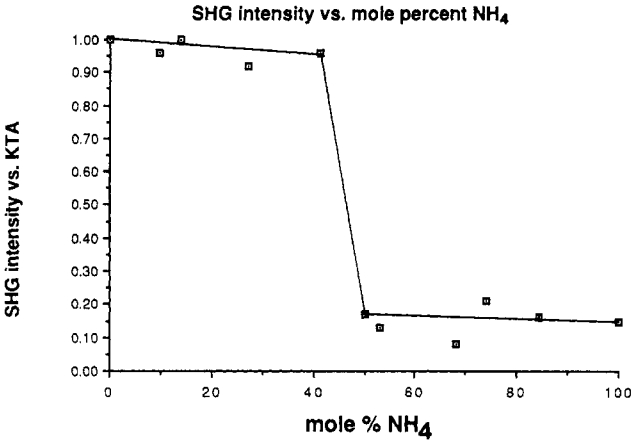

Figure 10. Compositional dependence of SHG intensity in the system $K_{1-x}(NH_4)_xTiOAsO_4$.

that there is a larger admixture of phosphorus orbitals into the framework oxygen levels than for arsenic. This gives a greater separation in the oxygen and transition-metal bands for the phosphate than for the arsenate. The virtual transition frequency ω_n between the oxygen and transition-metal-dominated bands which determines the value of β will contribute as $1/\omega_n$,[66] making KTA a better SHG material. The story is not complete, however, as evidenced by results obtained for $NH_4TiOAsO_4$ (NTA).

C. Ammonium Titanyl Arsenate (NTA).[45] $NH_4TiOAsO_4$ powder is readily obtained via the gel growth method. Crystals of NTA, however, are far more elusive: the hydrothermal method fails due to excess pressurization in the gold tubes, which causes leakage. Reaction between NH_4^+ and As(V) at elevated temperatures, yielding N_2(g), may be responsible. The only route to single crystals of NTA is therefore by ion exchange with KTA crystals. Since potassium is now being replaced with the larger ammonium ion, the consequent decrease in ion mobility slows the exchange rate considerably. Treating KTA crystals of sufficient size for single-crystal X-ray diffraction studies with molten NH_4NO_3 for 4 days results in only 50% exchange by mole of NH_4^+ for K^+. The resulting compound, $K_{0.5}(NH_4)_{0.5}TiOAsO_4$ or KNTA, has a powder SHG intensity only one-fifth that of KTA powder of similar crystal size.

If the SHG intensity of $K_{1-x}(NH_4)_xTiOAsO_4$ is plotted as a function of x (Figure 10), it is found that the powder intensity remains constant until the K:NH_4 ratio reaches 1:1. Thereafter, SHG intensity abruptly declines to approximately 20% of that of the less ammoniated materials. Since the SHG intensity of the corresponding phosphate NH_4TiOPO_4 (NTP) is on a par with KTP and KTA (Table VII), the loss of intensity in NTA cannot be an effect of NH_4^+ substitution alone, and incorporation of As into the framework must also be responsible.

Refinement of single-crystal X-ray data from $K_{0.5}(NH_4)_{0.5}TiOPO_4$ reveals no obvious changes in the Ti coordination environment of the titanium atom (Table VIII). Specifically, the short Ti=O bond distances, at 1.731 and 1.763 Å, do not differ significantly from those of KTA (1.735 and 1.770 Å, respectively). However, the selective siting seen in the KNTP and NHTP systems is not found in KNTA: K and NH_4 are distributed equally among the two nonequivalent cation sites. This is hinted at in the TGA plot of NTA, where it is seen that all of the weight is lost at nearly the same temperature, without the "break" in the weight loss curve found in NTP.[18]

The above results show that even more so than in KTA, the SHG intensity of NTA cannot be accounted for in terms of Ti–O distances alone. As the coordination of the ammonium ions in NTA is similar to that of the potassium ions in KTA, the influence of the cation on the optical nonlinearity of this material must be subtle indeed. We would suggest that in this case, hydrogen bonding between the NH_4^+ group and the more negative oxygen atoms in KTA (than in KTP) is stronger. This lowers the oxygen p band energies, thus increasing the effective bandgap. Inelastic and quasielastic neutron-scattering experiments are currently being used to pursue this line of thinking.[67] As shown below, guest cation effects can have a dramatic effect on SHG response, contrary to previous model hypotheses.

5. Guest Cation Effects on SHG Response. Within the $MTiOPO_4$ and $MTiOAsO_4$ systems there are several compounds whose powder SHG intensities are substantially or dramatically less than that of KTP. These include the compounds $(NH_4)_{0.5}H_{0.5}TiOPO_4$ (NHTP), $AgTiOPO_4$ (AgTP), and $NaTiOPO_4$ (NaTP). All of these compounds are at the edge of the KTP structure field, on the small-cation side. These materials have all been characterized structurally and are found to deviate from the KTP structure in ways that also emphasize the problems associated with neglecting cation bonding contributions in evaluation of SHG structure/property relationships. Additionally, these compounds are distinguished by the fact that they cannot be prepared by any direct combination of the oxides, and their synthesis demonstrates some of the more intriguing facets of the chemistry of KTP. These compounds therefore merit individual discussion.

A. Sodium Titanyl Phosphate (NaTP).[45] The polymorph of $NaTiOPO_4$ isomorphous with KTP, β-$NaTiOPO_4$, cannot be prepared directly in the solid state from stoichiometric quantities of the oxides, as the KTP phase space at this temperature ends at 65 mol % potassium. The region between 0 and 65 mol % Na is single phase and consists of a solid solution with the formula $K_{1-x}Na_xTiOPO_4$. The two-phase region between 65 and 100 mol % Na contains $K_{0.35}Na_{0.65}TiOPO_4$ and α-$NaTiOPO_4$ in varying proportion. The pure sodium-containing end member, α-$NaTiOPO_4$, is structurally related to the naturally occurring mineral $CaTiOSiO_4$ (titanite, or sphene).[68] This species is monoclinic, space group $P2_1/c$. It is centrosymmetric, and all of its second-order coefficients are therefore zero. Attempts to prepare β-$NaTiOPO_4$ from phosphate fluxes result in varying combinations of $NaTi_2(PO_4)_3$, α-$NaTiOPO_4$, and $Na_4TiO(PO_4)_2$,[69] depending on the temperature and Na/P ratio in the flux. The gel growth method is similarly unsuited for preparing the desired material: pure KTP results for Na/K ratios less than 1:1; beyond this point, a new, unidentified phase appears.

β-$NaTiOPO_4$ is prepared in powder or single-crystal form by treating KTP powder or crystals with a molten $NaNO_3$ flux at 350 °C. The ion exchange is rapid and complete and is presumably aided by the enhanced mobility of the smaller Na^+ ion. The resulting material is remarkably inert, as no significant phase transformation

(66) Actually, it will contribute as $1/(\omega_n^2 - 4\omega^2)(\omega_n^2 - 4\omega^2)$ for a situation where one charge-transfer term involving the virtual state $|n\rangle$ along one O–Ti–O axis makes the major contribution. The oscillator strengths (transition moments) also change with β as $\langle g|\mathbf{r}|n\rangle^2$.

(67) Rush, J. J.; Nicol, J.; Phillips, M. L. F.; Gier, T. E.; Stucky, G. D., manuscript submitted for publication.

(68) Donnay, J. D. H.; Ondik, H. M. *Crystal Data Determinative Tables*, 3rd ed.; National Bureau of Standards: Washington, DC, 1973; Vol. II, p M-49.

(69) Bamberger, C. E.; Begun, G. M.; Cavin, O. B. *J. Solid State Chem.* **1988**, *73*, 317–324.

to the α form takes place even after several days at 1050 °C. Lattice constants for the pure β-$NaTiOPO_4$ are given in Table VII. It is found that as Na replaces K in the $K_{1-x}Na_xTiOPO_4$ series, a and b decrease in equal proportion while c remains relatively constant. Ti–O distances from refinement of single-crystal X-ray data for $NaTiOPO_4$ are presented in Table VIII. Structural features of particular significance are the coordination numbers of Na(1) and Na(2), which are eight and four, respectively, and the Ti(1)–O(9)–Ti(2) bond angle, which at 130.8° is unusually small compared with 135.5° for the same angle in KTP. The close coordination of both Na(1) and Na(2) to O(9) is believed responsible. Close cation–O(9) coordination, also accompanied by perturbation of the Ti(1)–O(9)–Ti(2) bond angle, is seen in several other KTP isostructures as well and may be attributable to an unusual degree of basicity of this oxygen atom. The long-short character of the bridging Ti–O bonds, however, is unchanged on Na substitution.

Powder SHG intensity was measured on samples of $K_{1-x}Na_xTiOPO_4$ at varying values of x. It is found that the powder SHG intensity of β-$NaTiOPO_4$ is only approximately one-tenth that of KTP powder of similar crystallite size. As with KNTA, this loss of intensity cannot be accounted for in terms of Ti–O bond distances alone. It is postulated that alteration of the Ti(1)–O(9) bond polarizability caused by the short Na(1,2)–O(9) distance and the resulting loss of Ti(1)–O(9) bond valence is responsible for the low SHG intensity seen in NaTP, in addition to the bond angle reduction previously described. If virtual excited-state mixing predominantly involves the oxygen lone-pair electrons which are used in coordination to the sodium atom, substantial deviations in the Ti–O bond distances may not be observed, even though the SHG intensity is greatly modified. Cation coordination and bond-angle reduction are coupled with reduced SHG intensity in the AgTP and NHTP systems as well, which shall be detailed individually.

B. Silver Titanyl Phosphate (AgTP).[17] As with NaTP, $AgTiOPO_4$ must be prepared via ion exchange. Again, direct methods are unsuitable for preparing AgTP: sintering stoichiometric quantities of $AgNO_3$, $NH_4H_2PO_4$, and TiO_2 at 850 °C, for example, similarly results in the titanite isostructure α-$AgTiOPO_4$.[62] The gel growth technique also fails, yielding the insoluble and unreactive Ag_3PO_4. Highly crystalline $AgTiOPO_4$ powder may be prepared by treating KTP powder with molten $AgNO_3$ at 250 °C. This method, however, fails when applied to single crystals, as it results in translucent, badly twinned pieces. It is found that a lower melting flux, consisting of a 1:1 mixture by weight of $AgNO_3$ and $AgClO_3$ (mp = 143 °C), allows exchange into single crystals at milder temperatures (approximately 180 °C), over 48 h. While optical quality is retained, exchange is limited to the composition $Ag_{0.85}K_{0.15}TiOPO_4$. The mobility of the silver ions in AgTP and AgKTP is seen in its reactivity as well as its synthesis. For example, if AgKTP crystals are treated with a mild reducing agent such as hydrazine hydrate or hydroquinone, the surfaces of the crystals turn black from metallic silver.

Lattice constants and SHG intensities relative to quartz for both AgTP and AgKTP are presented in Table VII. The SHG intensities of these two compounds, at 5 and 7 times that of quartz, are 3 orders of magnitude less than that of the original KTP. Refinement of single-crystal X-ray data on the $Ag_{0.85}K_{0.15}TiOPO_4$ compound reveals no alteration of the Ti–O bond distances (Table VIII) that can directly account for this. Other interesting structural features of AgKTP include selective siting by the Ag and K atoms on the two crystallographically nonequivalent cation positions in the asymmetric unit. The occupancy of silver on Ag(1) is 100%, and 70% on Ag(2). The coordination numbers of Ag(1) and Ag(2) are four and eight, respectively. Also, Ag(1) is strongly coordinated to O(9) and, as in the case of NaTP, the Ti(1)–O(9)–Ti(2) bond angle is reduced, going from 135.5° in KTP to 129.5° in $Ag_{0.85}K_{0.15}TiOPO_4$. Again, it is suggested that lowering of the oxygen pπ band energy level with the concomitant decrease of the Ti–O bond polarizability is responsible for the loss of second-order nonlinearity, as observed by AgTP's low SHG intensity relative to KTP's.

C. Ammonium Titanyl Phosphate (NTP).[18] NH_4TiOPO_4 can be prepared as single crystals hydrothermally or as powder by using the gel growth technique. This system is unusual among the KTP family of isostructures in that it exhibits inclusion tunability in the gas phase rather than across a solid–liquid interface. When NTP is heated under vacuum, weight is lost in three steps. The first two steps correspond to desorption of NH_3 from the $NH_4(2)$ and $NH_4(1)$ sites, resulting in the intermediate compounds $(NH_4)_{0.5}H_{0.5}TiOPO_4$ and $HTiOPO_4$, respectively. $(NH_4)_{0.5}H_{0.5}TiOPO_4$ is a KTP isostructure (Table VII), while $HTiOPO_4$ is amorphous. The third weight loss step is due to loss of 1 mol of water per original NTP asymmetric unit to give a polymorph of $Ti_2P_2O_9$. When NHTP is treated with NH_3 or H_2O vapor, resorption occurs to give, respectively, NTP or $(NH_4)_{0.5}(H_3O)_{0.5}TiOPO_4$ (NOTP, Table VII).

On partial deammoniation to NHTP, powder SHG intensity declines to 6 times that of quartz, or one-thousandth that of KTP. Reammoniation to NTP or hydration to NOTP restores, in large measure, the original SHG. Single-crystal X-ray refinement on NHTP shows that the Ti(1)–O(10) bond distance has been lengthened from 1.718 Å in KTP to 1.901 A, resulting in loss of the long–short bridging Ti–O bonding in Ti(1). The coordination of Ti(2) is affected as well, with a switching of long and short bonding distances between Ti(2)–O(9) and Ti(2)–O(10) (Table VIII). The change in Ti coordination in NHTP, then, may partially explain the loss of SHG intensity in terms of Ti–O bond polarizabilities. Additionally, the Ti(1)–O(9)–Ti(2) angle is reduced to 127.4°. Since O(9) is adjacent to the now-vacant $NH_4(2)$ site, it is believed that protonation of this oxygen by the remaining hydrogen causes the change in bond angle, analogous to the change induced by coordination of Na in NaTP and by Ag in AgTP.

Ammonia loss is completely site selective; all of the remaining NH_4^+ ions are in the $NH_4(1)$ site, and the $NH_4(2)$ site is now vacant. Selective siting has also been observed in the KNTP system as well, in which ammonium ions are exclusively located in the $NH_4(2)$ site. Selective siting appears to be a general rule among $MTiOPO_4$ compounds, occurring in both the KNTP and KRbTP systems.[62] However, in the compound $KTiO(PO_4)_{0.5}(AsO_4)_{0.5}$, P and As occupy both of the tetrahedral sites to the same extent, so site selectivity is not the rule for all atom positions in the KTP structure.[62]

D. Thallium Titanyl Phosphate (TlTP). Either the flux growth[15] or hydrothermal methods are suitable for preparing $TlTiOPO_4$ crystals, and reaction conditions are very similar to those used to obtain KTP. SHG intensities measured for this material are similar to those obtained for KTP (Table VII), indicating that the nonlinearity of the host lattice is unaffected by Tl^+ inclusion. The mobility of the Tl^+ ions is comparable to that of potassium ions in KTP. This is evidenced by the facility with which

Tl may be exchanged onto KTP (001) surfaces to form optical wave guides (section 3.4). Owing to the increased refractivity of Tl versus K, the difference between the refractive index in the wave guide channel and the KTP substrate, Δn_{ij}, can reach values of up to 0.23, far exceeding Δn_{ij} values attainable by using Rb^+ (0.02) or Cs^+ (0.03).[13]

Single-crystal X-ray structure studies were undertaken on TlTP to determine whether the lone pair on Tl influences either the latter's coordination to the framework oxygens or the M–O bonding in the framework itself.[32] Tl–O bond distances reflect the stereochemical presence of the Tl^+ lone pair electrons. Tl(1) is coordinated to four oxygen atoms at distances of less than 2.85 Å (shortest Tl–O = 2.735 (4) Å) and two additional oxygen atoms at less than 3.15 Å. The remaining Tl–O distances are all greater than 3.25 Å. In KTP, on the other hand, eight K(1)–O distances are less than 3.1 Å (shortest K(1)–O = 2.717 (3) Å), even though the ionic radii of K^+ and Tl^+ differ by only 0.08 Å. Similarly Tl(2) has six nearest neighbors with Tl(2)–O bond distances less than 3.10 Å, with the remaining Tl–O distances greater than 3.20 Å. It is not clear at this time that the orientation of the Tl lone pairs in TlTP contributes substantially to the hyperpolarizability via strong directionality such as that seen in close-packed structures such as TlI.

6. Externally Induced Atomic Displacements and SHG

Chen[55] has pointed out that for nonisolated MO_6 units the SHG coefficient will depend entirely on the (MO_6) octahedra and their mode of distortion. It is of particular interest in this regard to monitor structure/property relationships within a given composition as a function of environmental changes which lead to measurable framework deformations. Three examples of this are (1) increasing temperature to take the ferroelectric KTP phase through the Curie transition to the paraelectric phase, (2) increasing pressure, which induces deformations leading to the antiferroelectric and paraelectric phases of KTP, and (3) using an applied electric field at low frequencies to monitor external electric field displacements. The first two of these applied to the KTP structural field are described below.

1. Thermal Displacements Leading to the Curie Temperature Transition. As discussed in section 3.3, KTP and several of its isostructures are ferroelectrics and undergo phase transitions at their respective Curie temperatures (Table III) to paraelectric phases. Yanovskii et al. surmised that these were displacive transitions, of nearly second order, and that the high-temperature phases belonged to the centric space group *Pnma*. That a transition to a centric space group occurs is corroborated by SHG data, which shows that SHG intensities are constant with temperature until the Curie temperature is approached, dropping to zero as T_c is crossed.[31]

We have performed high-temperature single-crystal neutron-diffraction experiments on a crystal of $TlTiOPO_4$ at both above and below T_c to directly determine the structure of the high-temperature phase (TlTP was selected for its low T_c; it is expected from the dielectric susceptibility and SHG studies that the behavior of other KTP isostructures is similar.[32] Data from a crystal heated to 650 °C reveal that the lattice symmetry has indeed changed, but to the centric space group *Pnan* rather than *Pnma*. There are still eight formula units per unit cell, but only one formula unit per asymmetric unit. The Ti and P atoms are now located on special positions, each with an occupancy of one-half. The net effect of the phase transition has been to move the Ti atoms to the center of their coordination spheres, such that the formerly long–short bridging Ti–O bonds have been replaced by bonds whose lengths are the average of the long and short Ti–O distances (Table VIII). Interestingly as the Curie transition point is approached at 500 °C, the bond alternation around Ti(1) is first lost as it is in $(NH_4)_{0.5}H_{0.5}TiOPO_4$. On the basis of this and several other observations the bond instability about Ti(1) appears to be greater than that associated with Ti(2). We suggest that the configuration and bonding at Ti(1) is particularly important in defining KTP NLO behavior. The high-temperature TlTP structure, then, represents the ultimate limit to which the KTP structure may be deformed in such a way as to reduce its nonlinear susceptibility.

2. Pressure-Induced Transitions. The pressure-drive ferroelectric → antiferroelectric → paraelectric transitions of KTP has been studied by Raman spectroscopy[70] by Kourouklis et al. Raman spectroscopy shows a first-order transition at 55 kbar which is driven by a low-frequency A_1 phonon mode at 56 cm^{-1} for the transition suggested as ferroelectric → antiferroelectric. The antiferroelectric → paraelectric transformation is assigned at slightly over 100 kbar. The structural mapping of this mode has been initiated by one of us (G.D.S.) and Bob Hazen of the Carnegie Geophysical Laboratory. The results obtained to date show a unique softening of the lattice as the phase transition is approached, which is reflected in the angular displacement of a titanium octahedron with respect to a phosphate tetrahedron. For example, a single Ti–O–P bond angle changes 6.1° between atmospheric pressure and 10 kbar. The next largest angular distortion is 1.9° between titanium octahedra, while all other angular changes are less than 1°.

7. Summary and Outlook

Referring again to Figure 8, experimentally we find that the trans-Ti–O distances involving the titanyl oxygen atoms are 1.94 Å for Ti(1) and 1.92 for Ti(2), while R_{av} for the cis titanyl atoms are close to 1.86 Å for the best SHG members of the KTP structural field, e.g., $KTiOPO_4$, $KTiOAsO_4$, and NH_4TiOPO_4. The maximum value in this curve as a function of distortion arises from the product of three transition moment terms, two of which are nonzero with the symmetrical geometry and one of which is zero. With increasing distortion the two nonzero terms decrease in value, while the remaining term rapidly increases. The maximum for the above three structures occurs very close to the experimentally observed value of $\Delta = 0.42$ (Table VIII). As noted above, Ti(2) appears to be less effective in contributing to the NLO response than Ti(1).

It is clear from structural studies on the compounds $(NH_4)_{0.5}H_{0.5}TiOPO_4$, $Ag_{0.85}K_{0.15}TiOPO_4$, β-$NaTiOPO_4$, and $K_{0.5}(NH_4)_{0.5}TiOAsO_4$ that earlier structure/property models do not predict SHG response in the KTP structure field. Inclusion tuning experiments show that it is not possible to treat the host framework independently of the cations and arrive at a reasonable model for all compounds. Likewise, it is evident that the differences in trans-metal–oxygen distances and the shortness of the Ti=O bond, while important, do not tell the whole story. The cations play a major role in defining the nonlinearity, and this

(70) Kourouklis, G. A.; Jayaraman, A.; Ballman, A. A. *Solid State Commun.* **1987**, *62*, 379.
(71) Avduevskaya, K. A.; Tananaev, I. V.; Mironova, V. S. *Izv. Akad. Nauk SSSR, Neorg. Mater.* **1965**, *1*, 894–9.
(72) Slobodanyk, N. S.; Nagornyi, P. G.; Skopenko, V. V.; Lugovskaya, E. S. *Zh. Neorg. Khim.* **1987**, *32*, 1724–8.
(73) Matvienko, E. N.; Yakubovich, O. V.; Simonov, M. A.; Belov, N. V. *Dokl. Akad. Nauk SSSR* **1979**, *246*, 875–8.

occurs by altering the polarizabilities of the bridging and framework Ti–O bonds without necessarily involving TiO_6 deformation.

The $KTiOPO_4$ structure field presents an unusual opportunity to evaluate structure/property relationships at the atomic level and to use this information to develop a predictive paradigm to create new nonlinear optic compositions in other metal oxide structural fields. The known isomorphs of KTP, of which there are already more than 40, have been made by both direct synthesis and inclusion tuning, in which cations are exchanged with a melt or, in the case of NH_4TiOPO_4 derivatives, are desorbed into or resorbed from the gas phase. The demonstrated possibility of *selective* siting for ion-exchangeable cations and the potential ability to do this for framework atoms add an unusual dimension to the value of the KTP structure field in correlating electronic and structural properties with NLO behavior. Replacing K and P with elements of greater or lesser atomic refractivity relocates the phase-matchable wavelengths in the resulting isomorphs. Replacing Ti with other elements shifts the LMCT absorption edge or eliminates it altogether, but probably at the cost of significantly reduced nonlinear susceptibility.

This multifaceted tuning is being exploited to investigate the finer details of the electronic and structural properties responsible for the unusually favorable NLO response in the KTP family. Already, KTA's electrooptic and nonlinear optic properties compare favorably with KTP's, and KTA may become more desirable than KTP for certain applications. It seems very probable that with the multidimensional compositional and structural space available to this family additional improvements in selected NLO properties will be obtained in the future.

Acknowledgment. This work was supported by the National Science Foundation. We also thank Drs. Nancy Keder and Bill Harrison for their assistance in preparing the crystallographic data.

Articles

Deep-UV Lithographic Response and Quantum Efficiency Calculations of Poly((trimethylsilyl)methyl methacrylate–(chloromethyl)styrene) Copolymers

M. J. Jurek,† A. E. Novembre,* I. P. Heyward, R. Gooden,‡ and E. Reichmanis

AT&T Bell Laboratories, Murray Hill, New Jersey 07974

Received March 21, 1989

The random copolymer comprised of (trimethylsilyl)methyl methacrylate, SI, and (chloromethyl)styrene, CMS, is known to function as a negative acting deep-UV and electron-beam resist. A range of copolymer compositions, from 0% CMS to 100% CMS, was synthesized to define a working range of sensitivity and weight percent silicon incorporation for use in bilevel applications. The Charlesby–Pinner relationship is used to determine the quantum efficiencies of cross-linking, Φ_{cl}, and chain scission, Φ_s, over the range of copolymer compositions. A preliminary study on the photochemistry of the poly(SI-CMS) copolymers as a function of composition, using either a pulsed KrF laser or a continuous-wave mercury vapor lamp, is presented.

Introduction

As integrated circuit technology becomes more sophisticated, greater demands are placed on the resist materials used in the lithographic pattern definition process. Necessary material requirements include sufficient sensitivity to exposure to ensure appropriate throughput and adequate resolution to enable VLSI device fabrication. Dry etching resistance has become increasingly desirable in pattern-transfer processes, especially for features <1 μm,[1] and for defining features on existing topography.

The incorporation of organometallic elements into resist materials as a mechanism for providing oxygen reactive ion etching resistance (RIE) has captured the attention of research chemists for several years. A wide range of organosilicon resist materials in which are organosilicon component has been incorporated into the polymer main chain as well as into pendent groups has appeared in the literature.[2-6] In addition to improved O_2 RIE resistance, organosilicon polymers allow a reduction in overall process complexity from a trilevel to a bilevel scheme. Unfortunately, this technology cannot be extended to most silyl-

† Current address: Ciba-Geigy Corp., Ardsley, NY.
‡ Current address: Dow Chemical, USA, Plaquemine, LA.

(1) Bowden, M. J. In *Materials for Microlithography*; Thompson, L. F., Willson, C. G., Frechet, J. M. J., Eds.; ACS Symposium Series No. 266; American Chemical Society: Washington, DC, 1984; pp 39–117.
(2) Taylor, G. N.; Wolf, T. M. *Polym. Eng. Sci.* **1980**, *20*, 1087.
(3) Kawazu, R.; Yamashita, Y.; Ito, T.; Kawomura, K., Ohno, S. *J. Vac. Sci. Technol.* **1986**, *B4*(1), 214.
(4) Reichmanis, E.; Smolinsky, G.; Wilkins, C. W. *Solid State Technol.* **1985**, *9*, 130.
(5) Novembre, A. E.; Reichmanis, E.; Davis, M. *Proc. SPIE Adv. Resist Technol. Proc. III* **1986**, *631*, 14.
(6) Tagawa, S. In *Polymers for High Technology: Electronics and Photonics*; Bowden, M. J., Turner, S. R., Eds.; ACS Symposium Series No. 346; American Chemical Society: Washington, DC, 1981; pp 37–45.

0897-4756/89/2801-0509$01.50/0